Master's thesis

NTNU
Norwegian University of Science and Technology
Faculty of Natural Sciences
Department of Physics

Maria Killingberg

Monte Carlo simulations and *in vitro* studies on the effect of crowder molecules on DNA condensation induced by CTAB

Master's thesis in Applied Physics and Mathematics
Supervisor: Rita de Sousa Dias
July 2020

NTNU
Norwegian University of
Science and Technology

Maria Killingberg

Monte Carlo simulations and *in vitro* studies on the effect of crowder molecules on DNA condensation induced by CTAB

Master's thesis in Applied Physics and Mathematics
Supervisor: Rita de Sousa Dias
July 2020

Norwegian University of Science and Technology
Faculty of Natural Sciences
Department of Physics

NTNU
Norwegian University of
Science and Technology

Abstract

Prokaryotic cells lack a nuclear membrane that separates the DNA from the cytosol, but the DNA is condensed into a structure called the nucleoid. The binding of nucleoid-associated proteins (NAPs) and macromolecular crowding (MMC) arising from the large concentration of macromolecules in the cell, are two mechanism believed to regulate DNA condensation in bacteria cells. Cationic surfactants, such as CTAB, self-assemble in the vincinity of DNA inducing its condensation, similarly to the condensing effect by some of the NAPs. While the majority of the published work dealing with MMC focus on neutral polymers, a large fraction of the macromolecules in the cytosol are negatively charged. In this work, the effects of negatively charged linear and branched polymers, as well as a neutral linear polymer (PEG), on DNA condensation induced by the cationic surfactant CTAB are investigated. The effects were investigated using coarse-grained Monte Carlo simulations, dye exclusion, electrophoretic mobility shift, and DNase protection assays.

Under the studied conditions, PEG weakly enhances DNA condensation by CTAB, particularly at high ionic strength. Negatively charged crowders enhance the condensation of DNA, due to the electrostatic repulsions. In the presence of CTAB, the crowders competes with the DNA for the binding to CTAB and DNA condensation is hindered. This opposing effect was found to be more evident for the linear than the spherical-like crowder, which was confirmed by coarse-grained Monte Carlo simulations. Increasing the salt concentration further highlighted these differences, with the dendritic polyanion nearly not affecting DNA condensation by CTAB.

These results suggest that negatively charged spherical-like macromolecules in the cytoplasm of bacterial cells do not interfere with, and can even potentially contribute to, the DNA condensation and nucleoid formation. Linear negatively charged macromolecules are expected to compete with the DNA for proteins with low specificity and affinity as well as other positively charged co-solutes, leading to the decompaction of DNA.

Sammendrag

Prokaryote celler mangler en nukleær membran som skiller DNA-et fra cytosol, men DNA-et er pakket til en struktur kalt nukleoiden. Bindingen av nukleoidassosierte proteiner og makromolekylær trengsel, som er forårsaket av den høye konsentrasjonen av makromolekyler i cellen, er to mekanismer som antas å regulere DNA-pakking i bakterieceller. Kationiske overflateaktive molekyl, slik som CTAB, samles i nærheten av DNA og induserer pakking, på samme måte som noen av disse nukleoidassosierte proteinene. Nøytrale polymerer blir ofte brukt ved undersøkelser av effekten av makromolekylær trengsel, men en stor del av makromolekylene i cytosolen er negativt ladet. Her ble effekten av negativt ladede lineære og forgrenede polymerer, og en nøytral lineær polymer (PEG), på DNA-pakking indusert av CTAB undersøkt. Dette ble undersøkt ved bruk av grovkornede Monte Carlo-simuleringer, og analyser av fargestoffekskludering, elektroforetisk mobilitetsforskyvning og DNase-beskyttelse.

Analysen viser at PEG svakt øker DNA-pakking med CTAB, spesielt ved høy ionestyrke. Negativt ladede trengselsmolekyler øker pakkingen av DNA på grunn av de elektrostatiske frastøtningene. I nærvær av CTAB konkurrerer trengselsmolekylene med DNA om CTAB, som senker interaksjonenen mellom DNA og CTAB, og hindrer pakking av DNA. Denne effekten ble funnet å være høyere for det lineære enn det sfæriske trengselsmolekylet, som ble bekreftet med Monte Carlo-simuleringer. Disse forskjellene ble enda mer fremhevet ved en økning av saltkonsentrasjonen, hvor den sfæriske polymeren nesten ikke påvirket pakkingen av DNA med CTAB.

Resultatene antyder at negativt ladede sfærisk-lignende makromolekyler i cytoplasma av bakterieceller ikke motvirker, og potensielt forbedrer pakking av DNA og dannelsen av nukleoiden. Lineære negativt ladede makromolekyler forventes å konkurrere mer med DNA om proteiner med lav spesifisitet og affinitet så vel som andre positivt ladede molekyler, noe som motvirker pakkingen av DNA.

Preface

This Master's Thesis concludes my studies at the program Applied Physics and Mathematics at the Norwegian University of Science and Technology.

I would like to thank my supervisor, Rita Dias, for exceptional support during the last year. Your guidance and scientific support in the project in the fall of 2019 and this thesis has been absolutely wonderful. I would also like to thank Gjertrud Maurstad for providing guidelines, materials and support when needed in the laboratory. Lastly, I want to thank my family for continuous support in every aspects of this work.

Unfortunately, the situation during the spring of 2020, which greatly affected the world in a tremendous way, also affected my work with this thesis. Limitations during this period restricted both access to the laboratory and access to material, which limited some of the experimental work that was intended.

Table of Contents

Chapter 1

Introduction

Early investigation of bacteria cells showed that they do not have a nucleus such as eukaryotic cells. The DNA in prokaryotic cells is contained in morphologically well-defined bodies, which were termed nucleoids, because they separate at cell division similarly to the nucleus in an eukaryotic cell [1]. The nucleoid lacks a membrane, but results from immersive refractometry have shown that there are variations in the refractive index between this structure and the cytoplasm indicating a phase separation between the cytoplasm and nucleoid. That is, the DNA is contained within a defined structure and does not spread throughout the entire cell [2, 3].

The genome of an *Escherichia coli* bacteria has 4.2 million base pairs, possessing a length of 1.4 mm when stretched, but fits into a nucleolar region of 1 μm [4]. Thus, the DNA must undergo some condensation in order to occupy a smaller volume within the cell, than that it occupies when free in solution. The mechanisms believed to aid in maintaining the structure of DNA and the nucleoid, are DNA association with nucleoid-associated proteins (NAPs), macromolecular crowding (MMC), DNA charge neutralization, and DNA supercoiling [5]. The full extent of the interplay between these forces is however not completely understood.

Investigation of DNA and its folding process is of importance in a range of fields. In molecular biology DNA condensation represents the importance of packaging the DNA in a way that allows for DNA replication and DNA transcription [6]. The degree of compaction mediates the extent of accessibility of the DNA sequences and is therefore indirectly responsible for the control of processes such as gene expression, recombination and repair. In eukaryotic cells the organization of the nucleosome (DNA-histone com-

plex) in hierarchical structures appears to provide a mechanism to modulate the stability of histone-DNA complexes and to facilitate or impede transcription. Conformational transitions and phase separation of DNA is a popular topic in polymer physics, given the rare possibility of working with polymers with monodisperse sizes. In medicine, DNA condensation play an important role in the delivery of DNA molecules to cells in gene therapy [4].

Diluted solutions are often used when investigating biochemical properties of a system to avoid or minimize the effects from nonspecific interactions or correlation effects. However, many biological media differ from this idealised setup due to the large concentration of macromolecules. The presence of these macromolecules, namely macromolecular crowding, is believed to significantly affect many biological, chemical and physical processes [7], such as protein stability [8] and nuclear function [9]. The cytoplasm of a prokaryote is a highly crowded environment. For example, the concentration of protein and RNA in *Escherichia coli* has been estimated to be 340 mg/mL [10]. Therefore, macromolecular crowding is believed to affect the maintenance of the nucleoid. Inert crowders are widely used to mimic such crowding effects, however RNA and many of the proteins found in the cytosol of *Escherichia coli* are negatively charged [11]. The aim of this thesis was therefore to investigate the effect of negatively charged linear and branched polymers on DNA condensation. As mentioned, the binding of nucleoid-associated proteins are believed to play an important role in DNA condensation. Many such proteins are amphiphilic and self-assemble in the presence of the DNA. In this work the cationic surfactant CTAB (cetyltrimethylammonium bromide) was used to mimic self-assembling nucleoid-associated proteins.

Monte Carlo simulation and *in vitro* studies were employed to investigate DNA condensation by cationic surfactants and the effect of crowding molecules on DNA condensation. Monte Carlo simulation is a molecular modeling method based on equilibrium statistical mechanics, which is used to study simplified molecular systems. This method was used to probe the effect of various crowders on DNA condensation induced by a model CTAB. *In vitro* studies were performed in addition, which included: (i) dye exclusion assays, where fluorescence spectroscopy is used to probe the exclusion of a fluorescent dye from the DNA when it condenses, and the consequent quenching of the fluorescence by the solution; (ii)

Electrophoretic mobility shift assays (EMSA), which utilises the change in mobility of DNA when it condenses; and (iii) DNase protection assays, performed to investigate the degree of protection given by the CTAB towards the digestion of the DNA by DNase, in the presence of crowding agents.

1.1 DNA

DNA is a polynucleotide with two strands that associate to form a double-helix structure [12]. Each nucleotide consists of a deoxyribose, a phosphate group, and one nucleobase. The nitrogen-containing nucleobase can either be thymine, cytosine, guanine or adenine. The nucleotides in a strand are connected by bonds between the phosphate and deoxyribose groups of consecutive nucleotides. The polynucleotides associate via hydrogen bonds formed between the nucleobases on either of the strands. The nucleobases associate according to the base pairing rules, which state that adenine binds to thymine, through two hydrogen bonds, and cytosine binds to guanine, through three hydrogen bonds.

The conformation of a polymer, which describes the relative location of the monomers in the polymer, depend on the flexibility of the chain, interactions between the monomers within the chain and interactions between the polymer and its surroundings (either other polymers or the solvent). In solution, polymers can interact with other elements over large length scales that affect their conformation and thermodynamic phase behaviour. The interaction between polymers and solvent, i.e. the solvent quality, determines the thermodynamic properties of the polymers, such as phase behaviour, rheological characteristics and their ability to associate with other molecules. These properties affect how expanded the polymers are in the solution. The polymer conformation is usually distinguished between three states. The compact state in which the chain is folded back on itself to minimize the contact between the polymer and solvent. The other extreme is when the polymer has a stiff, rod-like, conformation. However, most polymers, such as DNA and proteins in the denaturated state, have a less well-defined structure, called the random coil, in which the polymers have a large conformational entropy.

The stiffness of DNA, which affects how it interacts with other molecules and how easily it condenses, is a result of the mechanical properties of the DNA backbone, interactions between the strands and the stacking interactions between the bases [13]. The persistence

length is a measure of the stiffness of a polymer, which corresponds to the length where two segments keep their orientational correlation. Base sequence influences the stiffness due to the presence of either double or triple hydrogen bonds between the bases, where the latter has less rotational freedom. DNA and RNA in physiological conditions have a persistence length around 50 nm [13] and 5 nm [14], respectively. This highlights how the double-strand property of DNA affects its stiffness. The conformation is also a result of the fact that DNA is a negatively charged polyelectrolyte in a polar solvent. In the acid form, DNA looses its protons for nearly the entire pH range, and in the salt form, a number of its counterions dissociate from the negatively charged phosphate groups, which gives DNA an overall negative charge.

1.2 DNA condensation in prokaryotes

DNA condensation *in vitro* is defined as "the collapse of extended DNA chains into compact, orderly particles containing only one or a few molecules" [4], whereas DNA condensation in bacteria is defined as "adoption of relatively concentrated, compact state occupying a fraction of the volume available" [15]. This process, where a dramatic decrease in the volume occupied by the DNA occurs, is called on the simple molecule level the coil-globule transition. Electrostatic repulsions between DNA segments, loss of conformational entropy and the bending of the stiff DNA molecule opposes the process of DNA condensation. Condensation can be made more favourable by two mechanism, making the segment-segment interactions more favourable or making the DNA-solvent interactions less favourable.

1.2.1 Charge neutralisation and ion-ion correlation effects

DNA may be condensed by the presence of positively charged molecules. These can neutralise the DNA phosphate charges, decreasing the quality of the solvent or, if the positively charged molecules are multivalent, attractive interactions arise between DNA segments, the so-called ion-ion correlation effect [16]. Monovalent cations bind only transiently and form a diffuse electric double layer around the DNA. The Debye length, which is a measure of the range of electrostatic interactions in solution, changes with variations in the ionic strength of the solution. Increasing the ionic strength from 0.01 mM to 100

mM will drastically lower the electrostatic range from 96 to 0.96 nm (in water at 20 °C). The presence of salt will therefore lower the electrostatic repulsion between the DNA segments, hence lowering the persistence length [13]. A previous report has shown that above 0.01 M NaBr the persistence length is independent of salt concentration [17]. Monovalent cations do not by themselves induce DNA condensation, but can both aid DNA condensation, by screening the electrostatic repulsion between DNA segments, or oppose DNA condensation by affecting the interactions between DNA and positively charged species, particularly if these bind to DNA with low specificity.

Divalent metal ions, such as Mg^{2+} and Ca^{2+} are present in large amounts in the cytoplasm. Divalent cations bind more strongly to DNA and have been shown to induce DNA condensation [18, 19], depending on the cation and solution properties [4]. The structure of the condensed complexes also depends on the divalent cation [19]. Small and chain-like polyvalent cations induce DNA condensation by bridging and/or bending DNA segments. Results from streaming linear dichroism has shown that spermidine (3+), a polyamine usually found in bacterial cells, induce a cooperative change in size [20]. Other polyvalent cations such as spermine (4+) [21], $Co(NH_3)_6$ (3+) [22, 23] and polylysine have also been shown to induce DNA condensation.

1.2.2 Supercoiling

The DNA in bacterial cells is usually circular, which allows for supercoiling. This fundamental property of circular DNA causes under- or over-winding and is an important contribution to condensation of DNA in prokaryotes [24]. This was however not considered in this work.

1.2.3 Nucleoid-associated proteins

A large number of DNA-binding proteins have been identified as belonging in the nucleoid, and were therefore termed nucleoid-associated proteins (NAPs). NAPs were previously denoted histone-like proteins, not because they have a similar structure as histones, but rather due to their structural effect on DNA [25]. These proteins, e.g., H-NS, IHF, HU, Fis and Dps, are present in the cell and induce DNA bridging, bending and wrapping [26, 27, 28].

Cationic surfactants as a model for NAPs Surfactants, "surface active agents", are amphiphilic molecules that consist of two parts. One that is soluble and one that is insoluble in solution; when the solution is water the parts are termed hydrophilic and hydrophobic, respectively. Surfactants adhere to surfaces and interfaces due to the insolubility of the hydrophobic part, and in doing so lower the free energy of the phase boundary. At sufficiently high surfactant concentrations the surfactants form aggregates, also termed micelles, governed by the hydrophobic effect. The number of surfactant molecules in a micelle is called the aggregation number (N_{agg}). The concentration at which the surfactants start forming micelles is named critical micellar concentration (CMC). In the presence of polymers the surfactants start aggregating at a lower concentration, namely the critical aggregation concentration (CAC), which will depend on the properties of the polymer and surfactant.

The shape of the surfactant aggregate is governed by the shape of the surfactant, namely by the volumes of the hydrophilic (headgroup) and hydrophobic (tail) parts. The critical packing parameter (CPP) is used to determine the type of aggregate. This is given by CPP $= v/(l_{\mathrm{max}}a)$, where v is the volume of the tail, l is the tail length and a is the surface area of the headgroup. A spherical micelle is formed if the critical packing parameter CPP $< 1/3$ [29], as illustrated by Fig. 1.1. The headgroup of the surfactant can be anionic, cationic or nonionic, which will affect the CPP and interactions with other molecules. The area of the headgroup does not only depend on its van der Waals size, but also on hydration, ionic environment etc. Addition of salt will screen the electrostatic repulsions between surfactant headgroups, effectively reducing the area occupied by them and increasing the CPP, leading to the formation of cylindrical surfactant aggregates [30].

Due to their self-assembly properties, surfactants (in their multivalent aggregate form) can induce attractive interactions between DNA segments (ion correlation effects) [31, 32], bridging the segments and inducing DNA condensation. CTAB is not present in bacterial cells and is not believed to directly affect the stability of the nucleoid. However, many NAPs also possess amphiphilic properties, such as H-NS. H-NS is a dimer protein that, depending on the solution conditions (presence of Mg^{2+} [33]), self-assembles into protein oligomers along the DNA, hence inducing bridging of two DNA strands [34]. Due to this similar condensation mechanism, CTAB, which is easier to work with, can be used as a

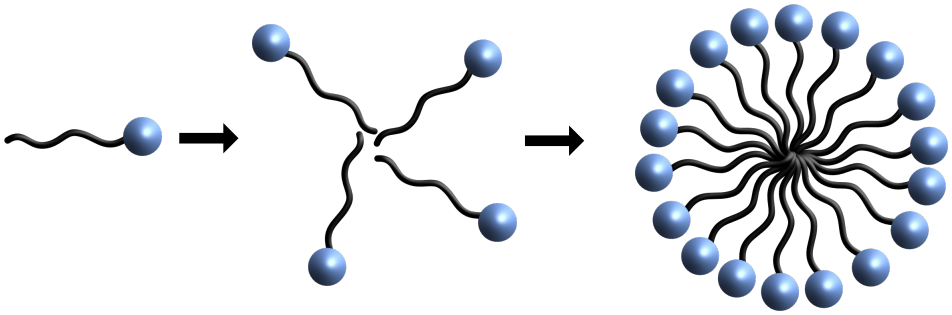

Figure 1.1: Illustration of the formation of spherical micelle by surfactants, with the hydrophilic headgroup (blue) and hydrophobic tail (black), in water. The right illustration is shown as a cross-section.

model for NAPs when investigating DNA condensation.

1.2.4 Macromolecular crowding

The large fraction of macromolecules in the cell reduces the space available to other molecules. MMC can thus aid in DNA condensation due to excluded volume effects, as reported in the 70s [35, 36]. The crowded environment lowers the conformational freedom of the molecules, favouring more compact conformations and hence aiding in DNA condensation [37]. MMC may also increase DNA condensation indirectly by enhancing the interactions between condensing ligands and DNA due to the crowded environment [38, 15].

Sedimentation studies of DNA in the presence of neutral polymers and salt have shown that DNA undergoes a cooperative transition from its solution structure to a compact state [35, 39], and this mechanism has been termed Ψ-condensation. The critical PEG concentration, defined as the PEG concentration needed to observe condensation of DNA, decreases with increasing degree of polymerization and salt concentration [36].

Seeing as a large fraction of the macromolecules in the cytosol of prokaryotes are negatively charged, electrostatic interactions from these macromolecules should play a role in the condensation of DNA [40, 41]. Many negatively charged polymers such as polyaspartic acid, polyglutamic acid [42, 43] and sodium polyacrylate [39] have shown to induce DNA condensation. The electrostatic repulsions between DNA and crowders could yield segregative phase separation of two concentrated phases, one rich in DNA and the other in crowders [5]. Such mechanism could explain the nucleoid phase separation

from the rest of the cytosol [44]. Negatively charged crowders are also vulnerable to environmental changes, where e.g. increased salt concentration will increase screening of the electrostatic interactions, with consequences to the MMC-effect.

Chapter 2

Monte Carlo simulation

2.1 Theory

Monte Carlo simulations are used to calculate ensemble averages of molecular systems. Refering specifically to DNA condensation in bacterial cells, the processes in such complex systems occur over length and time scales that are beyond the applicability of atomistic-level simulations. Coarse-grained simulations simplify the systems by clustering groups of atoms into new coarse-grained sites, which then interact in a more time efficient manner. Coarse-grained models aspire to reduce the complexity of the systems, while still be able to obtain their key physical properties.

Monte Carlo simulation relies on the generation of random configurations to calculate the ensemble averages for quantities that do not depend on the momenta [45]. That is, the simulations are limited to systems in equilibrium. In principle the configurations can be generated independently of each other, however the most common approach for generating a new configuration is to take the current one and randomly change the position of one particle. Such move is either accepted or rejected, based on the acceptance rules. The goal of this procedure, of which the Metropolis algorithm is one of the most used [46], is to improve the sampling of the configurational space that is relevant, while spending little time calculating configurations that contribute with zero to the Bolzmann factor. The acceptance rule of the Metropolis algorithm is done so that the system should evolve towards the equilibrium and once there, it should not leave it. In short this is done by accepting the new configuration if it has a lower energy or, in case there is an increase in the energy, if a random number, x, between 0 and 1 is lower than $\exp(\Delta U/k_{\mathrm{B}}T)$, where

$\Delta U = U_{\text{new}} - U_{\text{current}}$. The latter assumes that the systems move away from local minima.

2.2 Model

To investigate the effect of negatively charged crowders on DNA condensation induced by cationic surfactants, a simple model for a bacterial cell was adopted. The model consists of 5 types of chains and two types of counterions, as summarized in Table 2.1. The model for DNA consists of 120 negatively charged hard spheres (monomers) connected by harmonic bonds. The base pairs along the DNA are separated by 3.4 Å, which yields a linear charge density of $-8e$ per 13.6 Å. Therefore, the radius of the DNA monomers was set to $R_{\text{mon,DNA}} = 7$ Å, with a charge of $Z_{\text{mon,DNA}} = -8e$ placed in the center of the monomers.

To induce DNA condensation a model for CTAB was employed. The surfactant was

Table 2.1: Table presenting the particles in the model, their radius (R) and charge (Z).

	Particle type	# of particles	R /Å	Z
DNA	mon	120	7	-8
CTAB	head	1	4	1
	tail_1	1	2	0
	tail_2	1	2	0
PEG	mon	32	4	0
PMANa	mon	32	4	-1
PAMAM	mon_1	1	1	0
	mon_2	8	2	0
	mon_3	16	2	0
	mon_4	32	2	0
	mon_5	32	4	-1
Counterion (+)	ct_+	1	2	1
Counterion (-)	ct_-	1	2	-1

represented as a chain consisting of three types of monomers. The length of a CTAB molecule has been reported to be 2.2 nm [47], and is set to 20 Å in this model. The first monomer, termed head, has $Z_{\text{head,CTAB}} = +1e$ placed in the center of a sphere with radius $R_{\text{head,CTAB}} = 4$ Å, yielding a surface charge density of $0.5e/\text{nm}^2$. This monomer is connected to two subsequent neutral monomers, tail_1 and tail_2 with radius $R_{\text{tail}_1,\text{CTAB}} = R_{\text{tail}_2,\text{CTAB}} = 2$ Å.

To investigate the effect of crowder molecules, three different models were employed. Snapshots of the control systems with crowders are presented in Fig. 2.1. The first is a model for PEG, a neutral linear polymer, which is modeled by a linear chain of 32 neutral monomers, with $R_{\text{mon,PEG}} = 4$ Å. The second chain is a model for PMANa, which is a negatively charged linear polymer, modeled by a chain consisting of 32 negatively charged spheres. A charge $Z_{\text{mon,PMANa}} = -1e$ is placed in the center of the monomers, which have a radius $R_{\text{mon,PMANa}} = 4$ Å. The third crowder mimics PAMAM-OH generation 2.5 dendrimer, which is a branched polymer with 32 negative surface monomers. Though with a slightly larger radius of gyration, $R_G = 25$ Å, compared to the estimated R_G of 15 Å for a PAMAM dendrimer with 32 surface groups [48]. This crowder is modeled by a hierarchical structure with 4 generations. The central monomer is neutral and has a radius $R_{\text{mon}_1,\text{PAMAM}} = 1$ Å. The three inner generations consist of two monomers per branch with $R_{\text{mon}_2,\text{PAMAM}} = R_{\text{mon}_3,\text{PAMAM}} = R_{\text{mon}_4,\text{PAMAM}} = 2$ Å. The outer layer, i.e. generation 4, consists of one monomer per branch, with a total of 32 monomers. The monomers have a charge $Z_{\text{mon}_5,\text{PAMAM}} = -1e$ placed in the center of a sphere with radius $R_{\text{mon}_5,\text{PAMAM}} = 4$ Å.

The final particles in the systems are the corresponding positive and negative coun-

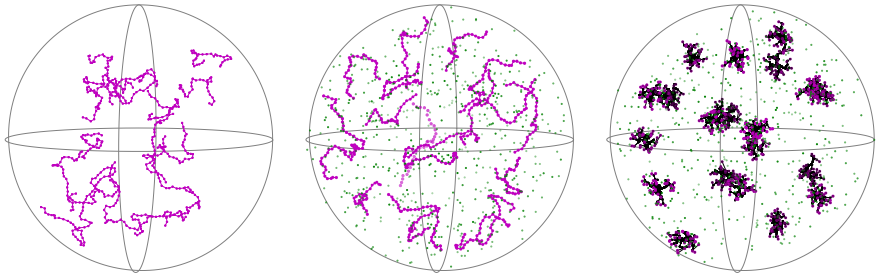

(a) P_0 **(b)** P_L **(c)** P_S

Figure 2.1: Representative snapshots of System (a) P_0, (b) P_L and (c) P_S, with PEG/PMANa (purple), PAMAM (black center and purple surface monomers) and positive counterions (green).

terions for all charged macromolecules in the systems, with $Z_{\text{ct}_+} = -Z_{\text{ct}_-} = +1e$ placed in the center of spheres with radius $R_{\text{ct}_+} = R_{\text{ct}_-} = 2$ Å.

The particles are contained within a sphere of $R_{cell} = 300$ Å. The solvent enters the model through its relative permittivity, $\epsilon_r = 78.4$, which equals the relative permittivity of water at 25 °C.

The total potential energy, U, of the system can be expressed as a sum of four terms,

the non-bonded potential energy U_{nonbond}, the bonded potential energy U_{bond}, the angular potential energy U_{ang} and a particle-cell wall potential energy U_{ext}. All interactions are pairwise additive.

$$U = U_{\text{non-bond}} + U_{\text{bond}} + U_{\text{ang}} + U_{\text{ext}} \tag{2.1}$$

The non-bonded potential energy of the system is given by

$$U_{\text{non-bond}} = \sum_{i<j} u_{i,j}(r_{i,j}) + \sum_{k<l} u_{LJ}(r_{k,l}) \tag{2.2}$$

where the first summation represents the electrostatic potential and extends over all particles. This electrostatic potential $u_{i,j}(r_{i,j})$, which also includes the hard-sphere repulsion, is given by

$$u_{i,j}(r_{i,j}) = \begin{cases} \infty, & r_{i,j} < R_i + R_j \\ \frac{z_i z_j e^2}{4\pi\epsilon_0\epsilon_r} \frac{1}{r_{i,j}}, & r_{i,j} \geq R_i + R_j \end{cases} \tag{2.3}$$

where z_i is the charge of particle i, $r_{i,j}$ is the distance between particles i and j, R_i is the radius of particle i, ϵ_0 is the vacuum permittivity and ϵ_r is the relative permittivity. Since the solvent is modeled as a continuum, the hydrophobic effect that leads to surfactant association in aqueous solution, is here replaced by a Lennard-Jones 6-12 potential applied between all $\text{CTAB}_{\text{tail}_2}$ monomers. This potential energy is given by

$$u_{LJ} = 4\epsilon \left[\left(\frac{\sigma}{r}\right)^{12} - \left(\frac{\sigma}{r}\right)^{6} \right] \tag{2.4}$$

where $\sigma = 6$ Å and $\epsilon = 3$ kT was employed. σ and ϵ are parameters that determines the equilibrium distance and strength of the attractive potential, respectively.

Particles belonging to a chain interact through a harmonic potential energy, U_{bond}, which is given by

$$U_{\text{bond}} = \sum_{c=1}^{N_c} \sum_{i=1}^{N_{mon,c}-1} \frac{k_{\text{bond}}}{2} (r_{c,i,i+1} - r_0)^2 \tag{2.5}$$

where k_{bond} is the force constant, $r_{c,i,i+1}$ is the distance between two connected monomers and r_0 is the equilibrium distance distance. The summations extends over all chains in the system (N_c) and all monomers of each chain ($N_{mon,c}$). The force constant for DNA, CTAB, PEG and PMANa are $k_{\text{bond}} = 0.4$ N/m, and equals $k_{\text{bond}} = 0.17$ N/m for PAMAM. The equilibrium distance for DNA, CTAB, PEG and PMANa is 15 Å, 7 Å, 9 Å and 9 Å,

respectively. For PAMAM, r_0 is 3 Å, 5 Å, 5 Å, 8 Å and 10 Å for $\mathrm{PAMAM}_{\mathrm{mon}_1}$ through $\mathrm{PAMAM}_{\mathrm{mon}_5}$, respectively.

The intrinsic stiffness of the chains is introduced by an angular potential energy, U_{ang}, which is given by

$$U_{\mathrm{ang}} = \sum_{c=1}^{N_c} \sum_{i=2}^{N_{mon,c}-1} \frac{k_{\mathrm{ang}}}{2}(\alpha_{c,i} - \alpha_0)^2 \tag{2.6}$$

where α_i is the angle formed by the position vectors $\mathbf{r}_{i+1} - \mathbf{r}_i$ and $\mathbf{r}_{i-1} - \mathbf{r}_i$, and α_0 is the reference angle (180 deg). The angular force constant of DNA, PEG and PMANa equals $k_{\mathrm{ang}} = 3.44 \times 10^{-24}$ J/deg^2, which correspond to a flexible chains, and $k_{\mathrm{ang}} = 1.66 \times 10^{-23}$ J/deg^2 was used for CTAB and PAMAM, which yields a stiff chain.

Finally, the confining external potential energy, U_{ext}, is given by

$$U_{\mathrm{ext}} = \begin{cases} \infty, & \mid r_i \mid > R_{cell} \\ 0, & \mid r_i \mid < R_{cell} \end{cases} \tag{2.7}$$

To investigate the effect of diverse crowders on DNA condensation 15 different systems were calculated, as summarised in Table 2.2. Systems are labeled according to which chains are present in the system, where D, C, P_0 (neutral polymer), P_{L} (linear polymer with negative charge) and P_{S} (spherical-like polymer with negative charge) indicate the presence of DNA, CTAB, PEG, PMANa and PAMAM, respectively. In general, systems with DNA have $N_{\mathrm{DNA}} = 1$ and systems with CTAB have $N_{\mathrm{CTAB}} = 960$, which were chosen such that $N_{\mathrm{head,CTAB}} Z_{\mathrm{head,CTAB}} / N_{\mathrm{mon,DNA}} Z_{\mathrm{mon,DNA}} = 1$. Systems with crowders have either $N_{\mathrm{PEG}} = 20$, $N_{\mathrm{PMANa}} = 20$ or $N_{\mathrm{PAMAM}} = 20$. The number of counterions, N_{ct_+} and N_{ct_-}, was varied so that all charged species contributed with the respective counterions.

2.3 Simulation details

Monte Carlo simulations were performed using the Metropolis algorithm in the canonical ensemble [49]. Each Monte Carlo step includes the trial displacement of a particle (including monomers) or chain. Translation of the chains and pivot-moves were employed for all chains in the systems. Slithering moves were also employed for DNA, CTAB, PEG and PMANa. Single-particle moves, which were tried 100 times more often than the other

Table 2.2: Summary of the systems studied in this work.

System	N_{DNA}	N_{CTAB}	N_{PEG}	N_{PMANa}	N_{PAMAM}	$N_{\mathrm{ct+}}$	$N_{\mathrm{ct-}}$
D	1	-	-	-	-	960	-
C	-	960	-	-	-	-	960
P_0	-	-	20	-	-	-	-
P_L	-	-	-	20	-	640	-
P_S	-	-	-	-	20	640	-
DP_0	1	-	20	-	-	960	-
DP_L	1	-	-	20	-	1600	-
DP_S	1	-	-	-	20	1600	-
CP_0	-	960	20	-	-	-	960
CP_L	-	960	-	20	-	640	960
CP_S	-	960	-	-	20	640	960
DC	1	960	-	-	-	960	960
DCP_0	1	960	20	-	-	960	960
DCP_L	1	960	-	20	-	1600	960
DCP_S	1	960	-	-	20	1600	960

type of trial moves, were applied for the counterions and all monomers of the chains. The moves may be rejected due to energy considerations, events that move the particles outside the simulation cell or due to hard-sphere overlaps.

The MOLSIM package (version 6.4.7) was used for the simulations [50]. All simulations included equilibrium runs, to reach the equilibrium of the systems, and production runs, which the results were calculated from. The number of simulation steps are presented in Table 2.3, and the lower values for some of the systems were due time restriction for this work. The statistical uncertainties were evaluated by block-averaging where one n_1-step constitutes one block [51].

To assess DNA condensation the radius of gyration, R_g, which is a measure of the chain extension, was calculated according to

$$\langle R_g^2 \rangle = \frac{\langle \sum_{i=1}^{N_{mon}} |r_i - r_{cm}|^2 \rangle}{N_{mon}} \tag{2.8}$$

where r_{cm} and r_i denotes the position of the center of mass of the chain and that of particle i, respectively.

To evaluate the aggregation of CTAB, cluster analysis was performed on the $\mathrm{CTAB}_{\mathrm{tail_2}}$. Two $\mathrm{tail_2}$ monomers, i.e. two CTAB chains, were considered part of the same cluster if the separation between these was less than $R = 2 \times (R_{\mathrm{tail_2,CTAB}} + R_{\mathrm{tail_2,CTAB}}) = 8$ Å, as

Table 2.3: Number of simulation steps for equilibrium and production runs calculated for each system.

System	Equilibrium run ($n_1 \times n_2$)	Production run ($n_1 \times n_2$)
D	30 × 40 000	100 × 40 000
C	30 × 40 000	50 × 40 000
P_0	30 × 40 000	50 × 40 000
P_L	30 × 40 000	50 × 40 000
P_S	30 × 40 000	50 × 40 000
DP_0	30 × 40 000	50 × 40 000
DP_L	30 × 40 000	60 × 40 000
DP_S	30 × 40 000	60 × 40 000
CP_0	30 × 40 000	50 × 40 000
CP_L	35 × 40 000	60 × 40 000
CP_S	45 × 40 000	60 × 20 000
DC	50 × 40 000	50 × 40 000
DCP_0	30 × 40 000	60 × 40 000
DCP_L	30 × 40 000	50 × 30 000
DCP_S	35 × 40 000	50 × 20 000

illustrated in Fig. 2.2.

To analyse the interaction between DNA and CTAB, contact analysis between DNA_{mon} and $CTAB_{head}$ was performed. These monomers were considered to be in contact if the distance between them was smaller than $R = 2 \times (R_{mon,DNA} + R_{head,CTAB}) = 22$ Å, as illustrated in Fig. 2.3.

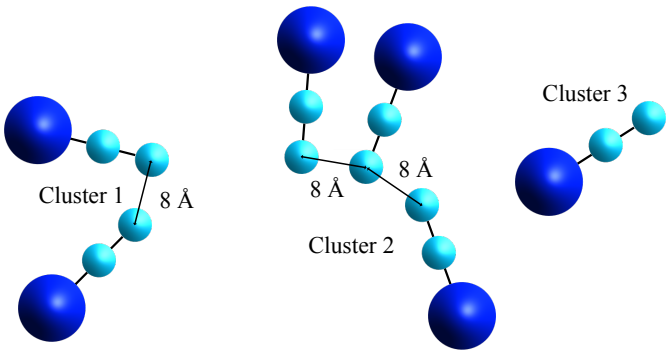

Figure 2.2: Illustration of the analysis calculating cluster sizes. Two CTAB chains were considered to be part of the same cluster if the distance between two $CTAB_{tail_2}$ was ≤ 8 Å.

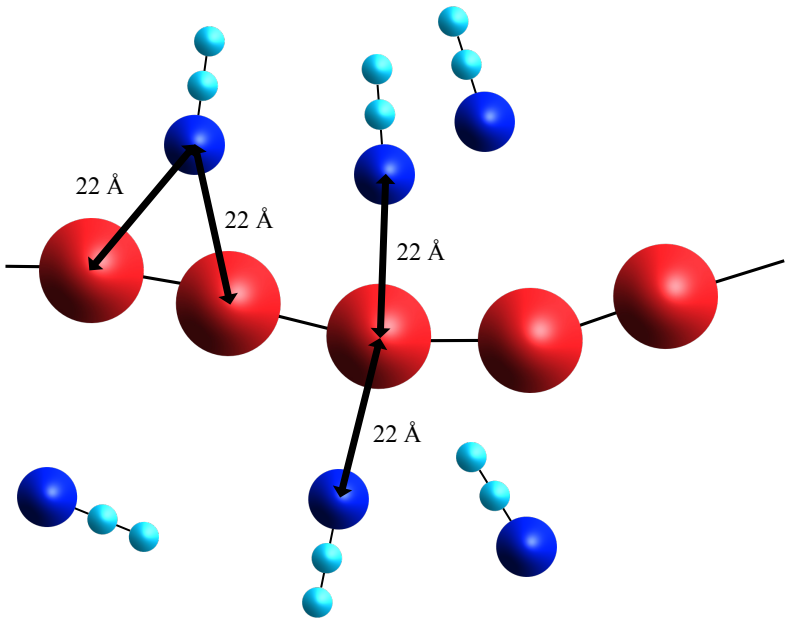

Figure 2.3: Illustration of the analysis calculating association between DNA_{mon} and $CTAB_{head}$. The particles were considered to be in contact if their separation was $\leq$ 22 Å.

2.4 Modification performed to the source code

Due to the large systems employed in this work, parts of the MOLSIM package needed to be slightly modified. The maximum allowed number of particles was increased. The routine used to employ slithering moves was changed to allow slithering of non-hierarchical chains in systems were hierarchical structures (PAMAM) were present but not subjected to the move type. The routine to calculate the contact probability between a particle type and the monomers of a chain, was originally designed to only allow calculation if one chain type was present in the system. The routine was therefore changed to allow calculations with several chain types present, and to allow the user to choose which chain type to use in the analysis.

Chapter 3

Experimental procedures

3.1 Materials and preparation of stock solutions

3.1.1 Materials

Tris(hydroxymethyl)aminomethane and hydrogen chloride for buffer preparation were purchased from Sigma Aldrich. 10 mg/mL DNA from salmon sperm (under 2 kbp) was purchased from Invitrogen and used as received. Cetyltrimethylammonium bromide (CTAB), the surfactant used to induce DNA condensation, and sodium bromide were obtained from Sigma Aldrich. Poly(ethylene glycol) Mn 6000 (PEG), used as neutral linear crowder, poly(methacrylic acid, sodium salt) Mw 4000-6000 (PMANa), used as a negatively charged linear crowder, and 10 wt.% PAMAM-OH generation 3.5 dendrimers in methanol, used as negative spherical crowder, were also purchased from Sigma Aldrich. GelStar (×10 000) used as dye in all *in vitro* experiments was obtained from Lonza. Agarose and 10× TBE-buffer used for the gel electrophoresis was acquired from Sigma Aldrich and Thermo Fischer Scientific, respectively. DNase I (RNase free) and 6× Tri-Track DNA Loading Dye were obtained from Thermo Fischer Scientific. Water used was deionized to a resistivity of 18.2 MΩ.cm (at 25°C).

3.1.2 Preparation of stock solutions

10 mM Tris-HCl buffer pH 7.4 was prepared and filtered with 0.2 µm Acrodisc Syringe Filters. Stock solutions of DNA, CTAB, NaBr, PEG, PMANa and PAMAM-OH were prepared in 10 mM Tris-HCl buffer.

Dialysis of PAMAM-OH

The PAMAM-OH dendrimers were received in methanol solution. Methanol has a lower dielectric constant than water and its presence would increase the electrostatic interactions between charged species (see Eq. 2.3). To avoid this, the methanol solution was exchanged with Tris-HCl buffer. Dialysis was performed by using the Pur-A-Lyzer midi 6000 dialysis kit MWCO 6-8 kDa purchased from Sigma Aldrich. Dialysis tubes were filled with PAMAM-OH dendrimer solution and placed in a beaker of Tris-HCl buffer, with 1000-fold the volume of the solution in the tubes. The PAMAM-OH solutions were dialysed for minimum 8 hours, depending on the volume, according to the recommendations of the manufactor. The dialysis tubes were weighted before and after dialysis to assess the final concentration of PAMAM-OH solution, which assumes that no PAMAM-OH dendrimers were lost in the dialysis process.

Concentration of PAMAM-OH solution

The concentration of received PAMAM-OH dendrimer solution was 81 mg/mL. The experiments where PAMAM-OH was used employs a procedure which requires a higher stock concentration. Therefore, the solution was concentrated, with the use of Amicon Ultra - 0.5 mL centrifugal filters. The procedure was executed by following the guidelines from the manufactor.

3.2 Fluorescence spectroscopy

Spectroscopy is the study of how molecules interact with and absorb electromagnetic radiation. Quantised electronic, vibrational and rotational states are available to molecules, and transitions between these states are allowed when electromagnetic radiation is absorbed or emitted, as shown in Fig. 3.1. Transitions between electronic states require radiation in the UV/Visible range, and functional groups of atoms in molecules that can absorb light in the UV/Visible range are called chromophores. These groups absorb light when the energy of the radiation corresponds to a change in the quantised electronic state of the molecule. When light is absorbed, the molecules undergoes a transition from a lower-energy state to a higher-energy state.

Re-emittance of absorbed radiation from a molecule in an electronically excited state

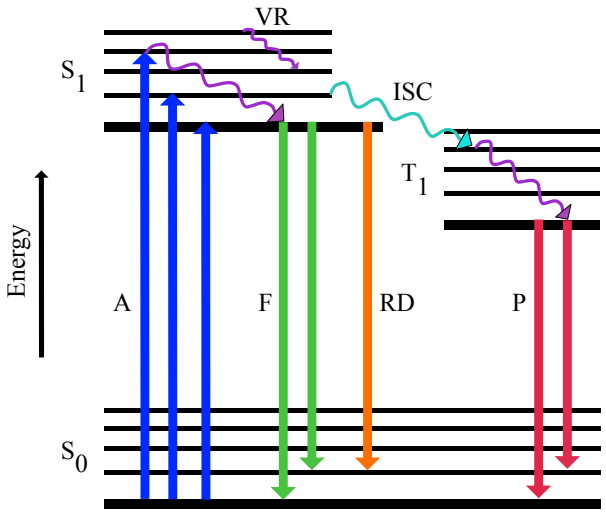

Figure 3.1: Jablonski diagram illustrating transitions between quantised electronic states (S_0 and S_1) by absorbing (A) and emitting electromagnetic radiation by fluorescence (F) and phosphoresence (P). The transition to the ground state can also occur via radiation-less decay (RD). Transition between vibrational states occur by vibrational relaxation (VR) and transition to an electronic state with different spin multiplicity (T_1) occur by intersystem crossing (ISC).

is called luminescence, which is divided into fluorescence and phosphorescence, as shown in Fig. 3.1. Molecules can also return to the ground state via a non-radiative process. These three processes comete and the one with the shorter lifetime for a particular type of molecule will be the one that prevails. Molecules that both absorb light and return to the ground state by fluorescence are called fluorophores. Fluorophores can be used as fluorescent probes to give information, depending on its properties, about a system. There exists naturally occuring fluorophores and fluorophores that are added to an otherwise non-fluorescent system, called intrinsic and extrinsic fluorophores, respectively. GelStar is an extrinsic fluorophore that shows a high fluorescent intensity when bound to DNA. When DNA condenses the dye is excluded and no longer bounds to DNA. Because water can accept a large quantum of electronic energy [52], the fluorescence is quenched by the aqueous solvent. Fluorescence spectroscopy can therefore be used to measure the decrease in fluorescence and thus to probe DNA condensation.

As it can be appreciated in Fig. 3.1, upon excitation to S_1, a molecule typically loses energy by heat by falling to the lower vibrational state of S_1 (vibrational relaxation), before it transitions to S_0. This means that the maximum of the emission spectrum is shifted towards higher wavelengths (lower energies) in relation to the absorption spectra.

3.2.1 Dye exclusion assay

To investigate the effect of crowder molecules on DNA condensation induced by CTAB, samples were prepared by adding 50 μL of 10 mM Tris-HCl buffer, 10 μL of 20 μg/mL DNA and 10 μL of ×100 GelStar to eppendorf tubes. Then the samples were left to equilibriate for 15 minutes. Afterwards, 10 μL of CTAB, with concentrations ranging from 0-500 μM, were added and the samples were left to equilibriate for 30 minutes. Then, 20 μL Tris-HCl, 20 μL of 125 mg/mL PEG, 20 μL of 125 (or 65) mg/mL PMANa or 20 μL of 125 (or 75) mg/mL PAMAM-OH dendrimers were added and the samples were left to equilibriate for 30 minutes. A reference sample was also prepared simultaneously using the same protocol, but replacing the volumes of CTAB and crowders with Tris-HCl buffer. The effect of crowding on DNA condensation induced by CTAB in high-salt environment was performed by preparing samples using the same procedure described above, but exchanging 10 μL of the initial Tris-HCl for 10 μL 1 M NaBr, and employing an additional waiting period of 30 minutes after the addition of DNA. A reference sample was prepared simultaneously using the same protocol, but replacing CTAB and crowders with Tris-HCl buffer.

To investigate the effect of adding crowder molecules to DNA, samples were prepared using the same protocol but replacing the CTAB solution with Tris-HCl buffer. Again, a reference sample for this procedure was prepared in parallel using the same method and also replacing the crowder molecules with Tris-HCl buffer. To investigate the effect of crowders on DNA conformation in high salt-concentration, samples were prepared using a similar procedure as described above, but exchanging 10 μL of the initial Tris-HCl for 10 μL 1 M NaBr, and employing an additional waiting period of 30 minutes after the addition of DNA. A reference sample was prepared simultaneously using the same protocol, but replacing PEG and PMANa, with Tris-HCl buffer.

To assess the interaction between GelStar and the various components used in this work, negative controls were prepared with GelStar alone and GelStar in the presence of CTAB, PEG, PMANa or PAMAM-OH, with or without NaBr. The samples were prepared according to the protocols described above but replacing the unwanted components with Tris-HCl buffer. A reference sample with DNA and GelStar was prepared simultaneously.

The samples were transferred to a BD Falcon 384 black well plate obtained from

Thermo Fisher Scientific and the fluorescence emission was measured using a Spectramax I3X well scanner. The excitation wavelength was 493 nm and the emission intensity was measured from 520 nm to 620 nm with intervals of 5 nm.

3.3 Gel electrophoresis

Gel electrophoresis is a method which separates charged molecules based on their size, by applying an electric field over a gel in which the molecules, if charged, migrate. The force experienced by the molecules in the electrical field is given by Coulomb's law

$$F = ZeE \tag{3.1}$$

where Z is the positive or negative number of charges, e is the electron charge and E is the electrical field (in units of potential per centimeter). In free solution electrophoresis, the net force on the molecule must be zero when there is steady motion, which gives

$$fv = ZeE \tag{3.2}$$

fv is the force that opposes motion due to friction, where f is the frictional factor and v is the velocity of the molecule. Rearranging one gets the electrophoretic mobility, U:

$$U = \frac{v}{E} = \frac{Ze}{f}, \tag{3.3}$$

where $f = 6\pi\eta a$, as stated by Stokes's law, can be used if the molecule is spherical. a is the particle radius and η is the solvent viscosity.

Electrophoretic mobility shift assay, which is mainly used to separate DNA, uses a gel with such concentration that it acts as a molecular sieve. A large molecule cannot move as easily through the network as it can in free solution. In DNA, the charge is proportional to its length and thus the electrophoretic mobility in solution is essentially independent of the molecular weight. The separation of the molecules on the gel depend therefore entirely on the molecular sieving, on the basis of their molecular sizes. A series of DNA fragments with known molecular weights, called ladder, are used to estimate the molecular weight of unknown DNA molecules [53]. In this work gel electrophoresis is used instead to assess the interaction of DNA with CTAB. Upon the binding of CTAB to DNA three phenomena

occur: (i) the DNA condensed into a smaller complex involving one or few molecules with a hydrodynamic radius that is smaller than that of free DNA. This is expected to occur for low CTAB concentrations and is more evident for large DNA molecules [54], and it would lead to an increase in the electrophoretic mobility (see Eq. 3.3); (ii) larger DNA-CTAB aggregates are formed and the combined increase in molecular weight and radius leads to a decrease in mobility; and (iii) the charge of the DNA decreases also leading to a decrease in mobility [55]. Within the conditions of this work, phenomena (ii) and (iii) are expected to be the most dominant, thus the differences in migration makes it possible to assess DNA condensation by this method.

DNase protection assay is used to assess the degree of protection given by the different components and their mixture to the DNA, towards DNase activity. DNase I is an enzyme that digests DNA by cleaving the covalent bonds between nucleotides. In addition to the effect observed in EMSA as stated above, two phenomena may occur: (i) digestion of a DNA molecule leads to an increased velocity trough the gel which makes it possible to assess the DNase activity; (ii) shorter DNA strands (due to digestion by DNase) allows for neutralisation of DNA-CTAB complexes to occur at lower concentrations of CTAB.

3.3.1 Sample preparation

Samples were prepared by adding 30 μL of 10 mM Tris-HCl buffer, 5 μL of 250 μg/mL DNA and 5 μL of CTAB, with concentrations ranging from 0-8 mM, and leaving the samples to equilibriate for 30 minutes. Afterwards, either 10 μL of 125 mg/mL of PEG, 10 μL of 125 mg/mL PMANa or 10 μL of 125 mg/mL PAMAM-OH dendrimers were added, and the samples were left to equilibriate for 30 minutes. Reference samples were prepared simultaneously using the same protocol, but replacing the volumes of crowders with Tris-HCl buffer. To investigate the effect of ionic strength in these systems, samples were prepared following the same procedure but exchanging 5 μL of the initial Tris-HCl with 5 μL 1 M NaBr, and employing an additional waiting period of 30 minutes after the addition of DNA. Reference samples were prepared in parallell following the same protocol, with the exception that Tris-HCl buffer was added instead of PEG, PMANa or PAMAM-OH.

3.3.2 Electrophoretic mobility shift assay

0.8 % agarose gels were prepared by mixing 0.8 g agarose with 100 mL of 1× TBE-buffer and heating up the solution to dissolve the agarose. After the solution had cooled down, 5 µL of ×10 000 GelStar was added and the solution was transferred to a VWR casting tray and left to settle for 60 minutes. The gel was placed in the electrophoresis chamber and 1× TBE-buffer was added until the gel was covered. 10 µL of each sample, prepared according to the protocol described in Section 3.3.1, were mixed with 2 µL 6× loading dye, and 10 µL of this solution was placed in a well in the gel. The gels were ran for 50 minutes at 90 V, applied by a VWR 250 V Electrophoresis Power Supply. After the run, the gels were visualized using a Benchtop 3UV Transilluminator at 365 nm.

3.3.3 DNase protection assay

2 µL of 2 U/µL DNase I was added to the samples, prepared as described in Section 3.3.1. These were then incubated at 37°C for 30 minutes, followed by 10 minutes at 70°C to induce the denaturation of the DNase and stop the digestion reaction. 10 µL of the samples were mixed with 2 µL 6× loading dye and 10 µL of these solutions were moved to the wells in 0.8 % agarose gel with GelStar, which was ran and analysed using the procedure described in Section 3.3.2.

Chapter 4

Results

In the following sections, results from Monte Carlo simulation, dye exclusion assay, EMSA and DNase protection assay are presented, to probe the effect of crowder with different properties on DNA condensation induced by CTAB.

4.1 Monte Carlo simulation

4.1.1 Conformation of DNA

The probability distribution of the radius of gyration, $P(R_G)$, of model DNA in the absence and presence of crowders are shown by the solid lines in Fig. 4.1. In System D, it can be seen that the size distribution of the DNA is wide and centered around 195 Å. In the presence of neutral polymers (System DP_0), the size distribution has a similar shape as in System D, however it is slightly shifted towards the right, i.e. towards larger sizes. In the presence of linear charged polymers (System DP_L) the size distribution is wider, shifted towards lower values, and centered around 185 Å. For spherical crowders (System DP_S), the size distribution of DNA has a similar shape as in System DP_L, however the distribution is slightly shifted to the left, centered around 180 Å. Representative snapshots of these systems are presented in Fig. 4.2a-4.2d.

The radius of gyration of the model DNA with CTAB in the absence and presence of crowders are shown by the dashed lines in Fig. 4.1. In System DC, the size distribution is more narrow than observed for System D and centered at around 100 Å. Addition of neutral linear crowder (System DCP_0) shifts the size distribution towards larger sizes, compared to System DC. The distribution is very narrow and centered around 145 Å.

$P(R_G)$ in System DCP_L is slightly shifted towards the right and has a broader distribution compared to System DC. In System DCP_S, the distribution has a peak at approximately similar sizes as in System DC, however the distribution is slightly shifted towards lower values. Representative snapshots of these systems are presented in Fig. 4.2e-4.2h.

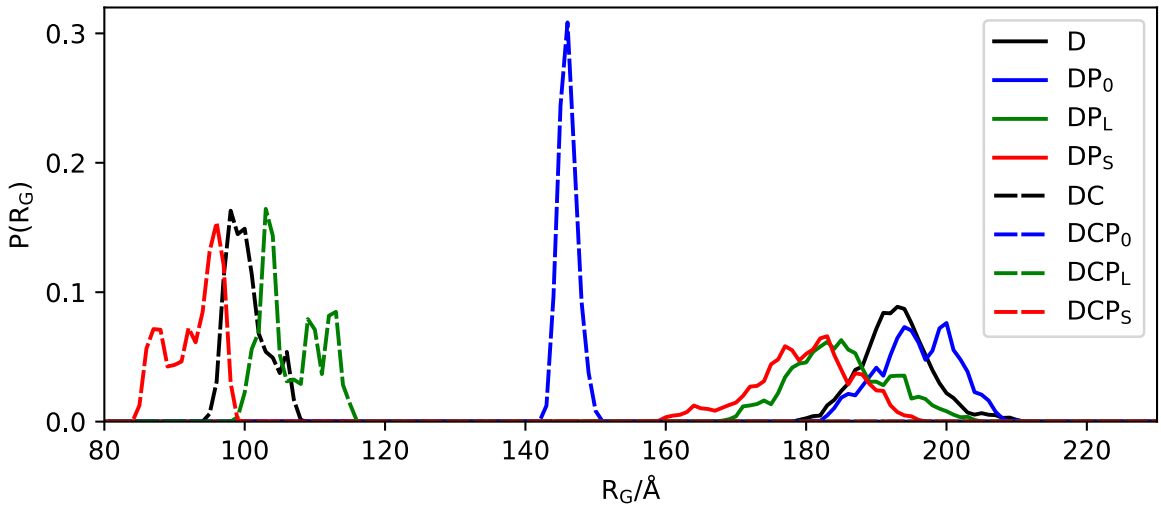

Figure 4.1: Probability distribution of radius of gyration, $P(R_G)$, of model DNA in System D, DP_0, DP_L and DP_S, DC, DCP_0, DCP_L and DCP_S, as indicated in the figure (see Table 2.2 for details on the systems).

4.1.2 DNA-CTAB association

The radial distribution functions (rdf) of the DNA_{mon} – $CTAB_{head}$ pairs in the absence and presence of different crowders are presented in Fig. 4.3. Starting with System DC it can be seen that the rdf is zero up to separation of $R_{mon,DNA}+R_{head,CTAB} = 11$ Å. A sharp increase at 11 Å indicates that the CTAB headgroups associate strongly with the DNA monomers. The $g(r)$ of Systems DCP_0, DCP_L and DCP_S have a similar shape as System DC, however the maximum decreases from 145 to 143, 128 and 116, respectively, indicating a weakening of the interaction. Contact analyses between $CTAB_{head}$ and DNA_{mon} are presented in Fig. 4.4. This analysis shows the number of $CTAB_{head}$ at a distance lower than 22 Å from each DNA_{mon} in the DNA chain. In System DC, the distribution of CTAB headgroups shows approximately 12 peaks along the DNA chain, with slightly higher peaks in the center of the DNA chain. In System DCP_0, there is no significant presence of peaks along the DNA chain, however a stable value of approximately 12 CTAB headgroups are in

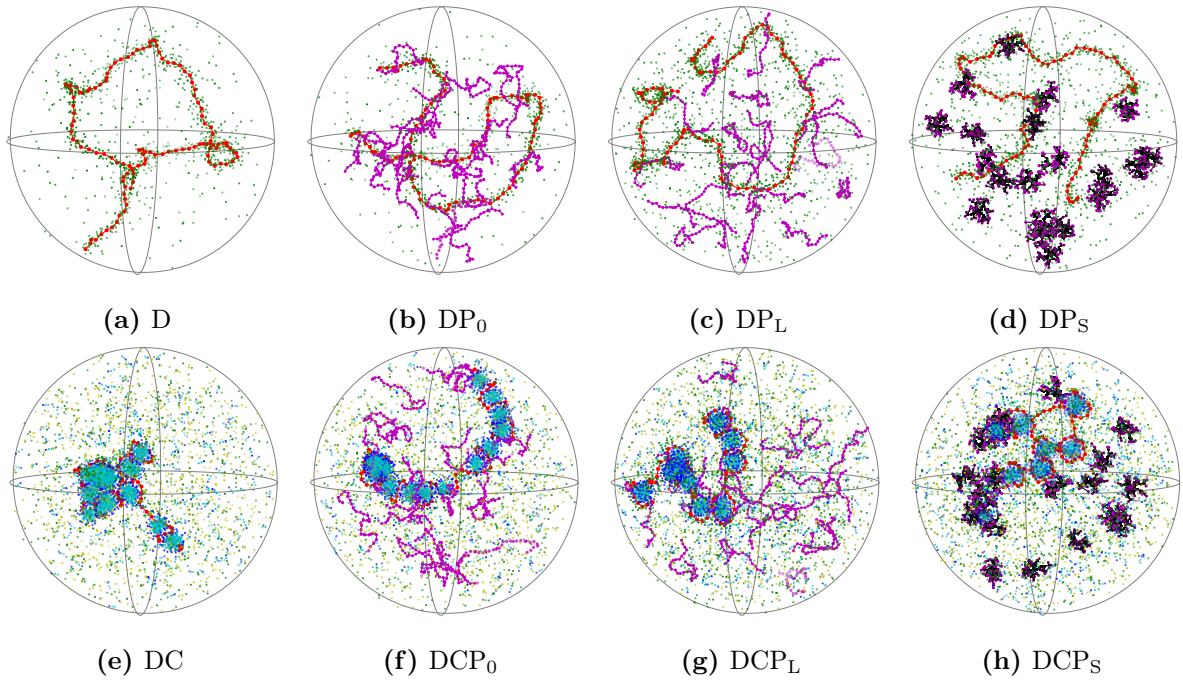

(a) D **(b)** DP_0 **(c)** DP_L **(d)** DP_S

(e) DC **(f)** DCP_0 **(g)** DCP_L **(h)** DCP_S

Figure 4.2: Representative snapshots of System (a) D, (b) DP_0, (c) DP_L, (d) DP_S, (e) DC, (f) DCP_0, (g) DCP_L and (h) DCP_S, with DNA (red), CTAB (blue head and cyan tail), PEG/PMANa (purple), and PAMAM (black center and purple surface monomers). The positive and negatively charged counterions are represented using green and yellow particles, respectively.

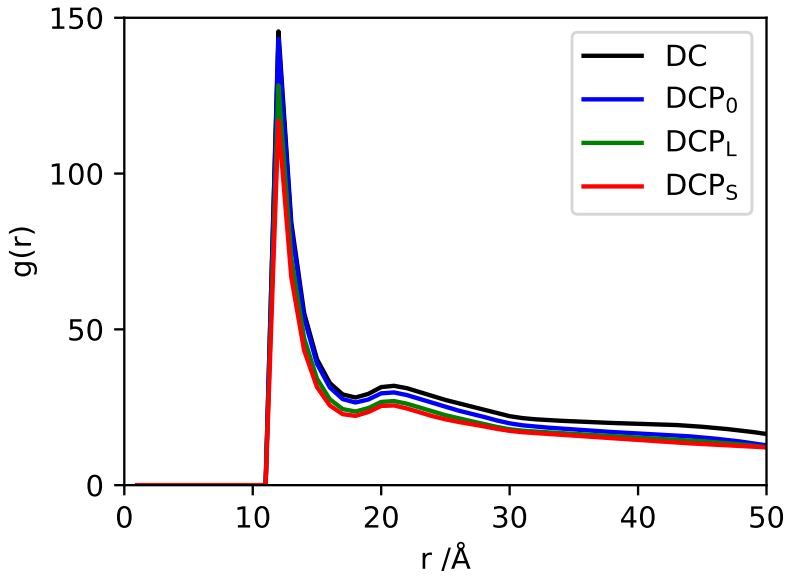

Figure 4.3: Radial distribution functions, $g(r)$, of DNA_{mon} – $CTAB_{head}$ particle pairs in System DC, DCP_0, DCP_L and DCP_S, as indicated in the figure (see Table 2.2 for details on the systems)

contact with each DNA monomer. In Systems DCP_L and DCP_S, the contact profiles look somewhat different, with the number of CTAB headgroups being approximately 10 along the DNA chain, but with occasional maxima and minima ranging from 1 to 15 CTAB

headgroups, depending on system and monomer index.

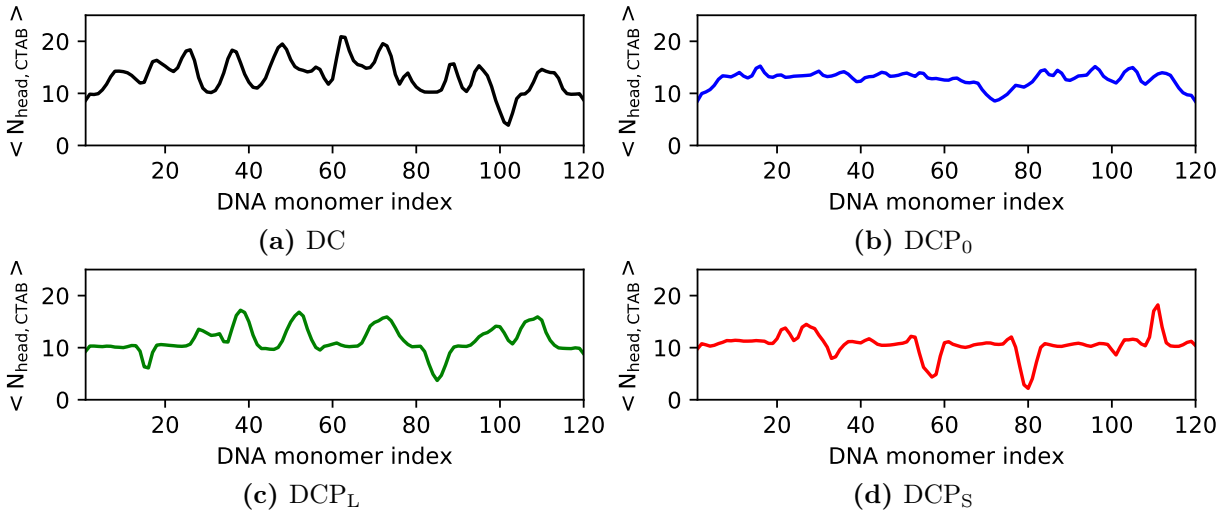

Figure 4.4: Average number of CTAB headgroups at a distance lower than 22 Å from a DNA monomer, versus the DNA monomer index, for Systems (a) DC, (b) DCP_0, (c) DCP_L, and (d) DCP_S.

4.1.3 CTAB self-assembly

The rdf of $CTAB_{tail_2}$ – $CTAB_{tail_2}$ pairs, in the systems with CTAB alone and in the presence of crowders, are presented in Fig. 4.5a. Systems C and CP_0 have a $g(r)$ with an approximately constant value of 1 above 8 Å, except for a slight maximum at 6 Å where $g(r)$ equals 10, consistent with the equilibrium distance of the LJ potential. Systems CP_L and CP_S also have a maximum at 6 Å where $g(r)$ equals 195 and 190, respectively, followed by two other maxima at 11 and 16 Å, which indicates a large degree of order. This can be seen in the representative snapshots of these systems, presented in Fig. 4.6a-4.6d.

The rdf of $CTAB_{tail_2}$ – $CTAB_{tail_2}$ pairs, in the presence of DNA, and with the further addition of crowders, are presented in Fig. 4.5b. It can be seen that all four systems show similar results with the $g(r)$ increasing sharply above 4 Å (sum of the hard-sphere radius) and with a maximum at 6 Å, also followed by maxima at 11 and 16 Å. System DC shows the largest CTAB concentration, followed closely by Systems DCP_0, DCP_L and DCP_S. Comparing panels a and b, it is clear that stronger CTAB association occurs in the presence of the DNA. Results from the cluster analysis on $CTAB_{tail_2}$ are presented in Fig. 4.7. In all systems there is a very high probability of finding individual surfactants ($N_{agg} = 1$) and small clusters with sizes ranging from 2 to 7. In order to best assess the

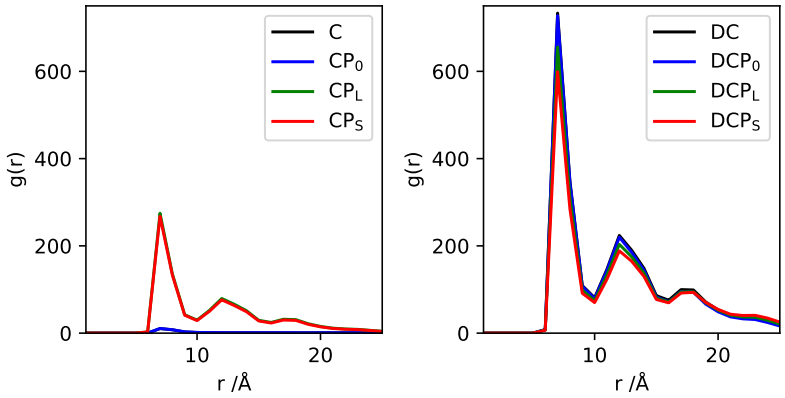

(a) **(b)**

Figure 4.5: Radial distribution functions, $g(r)$, of CTAB – CTAB in (a) systems with CTAB in the absence and presence of crowders, and in (b) systems with CTAB and DNA in the absence and presence of crowders, as indicated by the labels.

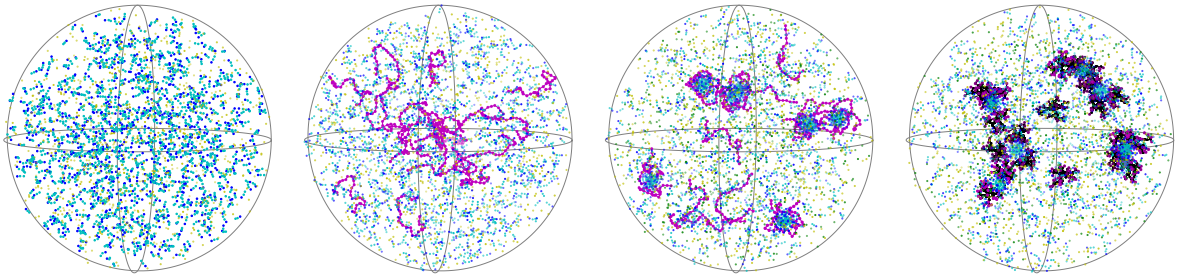

(a) C **(b)** CP_0 **(c)** CP_L **(d)** CP_S

Figure 4.6: Representative snapshots of System (a) C, (b) CP_0, (c) CP_L and (d) CP_S, with CTAB (blue head and cyan tail), PEG/PMANa (purple), PAMAM (black center and purple surface monomers). The positive and negatively charged counterions are represented using green and yellow particles, respectively.

difference between the systems, this peak is not fully shown. In Systems C and CP_0 there is zero probability of finding aggregates with numbers larger than 7. For System CP_L the distribution indicates the formation of micelles with aggregation numbers ranging from 30 to 60 CTAB molecules. System CP_S has a similar probability distribution as System CP_L, but also shows some probability of finding smaller micelles with aggregation numbers around 10.

The addition of DNA changes significantly the aggregation behaviour of CTAB. In System DC the aggregation number now ranges between 20 to 80, with a slightly higher probability of aggregation numbers above 40. System DCP_0 shows a narrower size distribution shifted towards smaller aggregation numbers when compared to System DC. The presence of linear negatively charged polymer leads to a smaller number of larger

aggregates, ranging from 40 to 90, while spherical-like negatively charged crowders show, besides the large peak for small sizes, a probability of finding aggregates of two different sizes, namely 10-48 and 70-100, where the latter has a higher probability compared to the former.

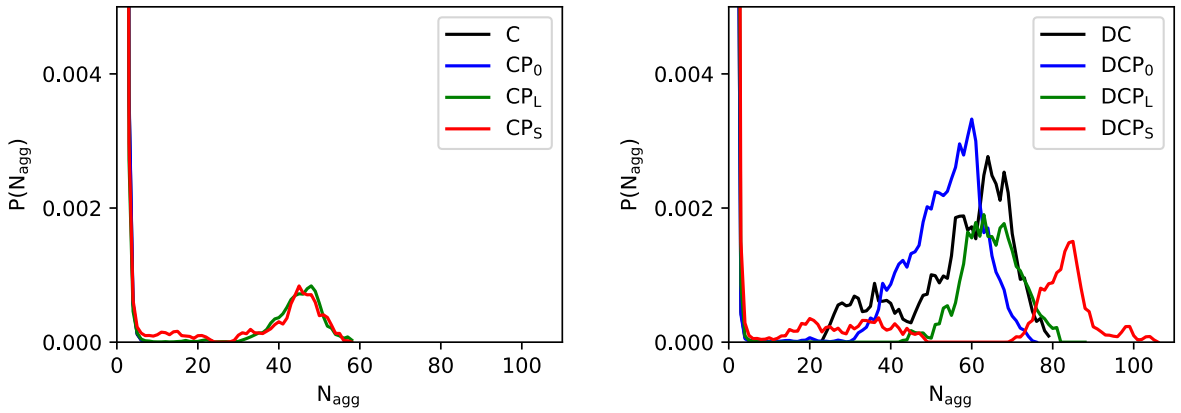

(a) **(b)**

Figure 4.7: Probability distribution of CTAB aggregation numbers in systems with (a) CTAB in the absence and presence of crowders, and (b) DNA + CTAB in the absence and presence of crowders, as indicated by the labels.

4.1.4 Effect of crowders on DNA-CTAB interaction

The rdfs involving the crowders are presented in Fig. 4.8. The top row refers to the crowder – crowder pairs and is based on the separation between the centers of mass, r_{CM}, of the PEG pairs and the PMANa pairs, and based on the distances between two $\mathrm{PAMAM}_{\mathrm{mon_1}}$ (i.e. the central monomer) for PAMAM pairs. Considering the $g(r)$ for PEG – PEG pairs (panel a), it can be seen that the distribution is similar to all studied systems, showing an initial depletion at short separations, followed by a shallow peak at 100 Å.

The rdfs of the PMANa – PMANa polyanions are shown in Fig. 4.8b. System $\mathrm{P_L}$, with only PMANa, shows a more evident depletion effect between chains than System $\mathrm{P_0}$ in panel (a) due to the repulsion between chains, with the broad peak now showing a maximum at around 160 Å, and $g(r) = 0$ for radial distance below 75 Å. The addition of DNA (System $\mathrm{DP_L}$) leads to a shift in the distribution toward slightly lower values, probably due to crowding effect. Further addition of CTAB (System $\mathrm{DCP_L}$) does not seem to affect the distribution of the linear negatively charged crowders within the simulation

cell. System CP_L is, however, markedly different. It is clear that CTAB induces PMANa association, as seen by the maximum at 0 Å (recall that the analysis is conducted for the CM in this system) with $g(r) = 25$ (not shown for best readability), and a second maximum at 40 Å with $g(r) = 9$.

The rdfs of PAMAM – PAMAM dendrimers presented in Fig. 4.8c, show similar trends. Systems P_S and DP_S show a repulsion between the PAMAM with a broad peak starting at 100 Å and showing a maximum at 160 Å. Again the presence of DNA (System DP_S) leads to a shift in the distribution toward lower values, compared to System P_S. Addition of CTAB to the dendrimers (System CP_S) also induces the association of the dendrimers. Since the analysis is conducted taking into account the central monomer the first maximum arises at $r \sim 70$ Å. A second defined peak is present around 130 Å indicating the aggregation of more than two dendrimers. A third peak is visible for larger separation, that overlaps with that of System P_S, referring to dendrimer pairs that are not associated. Finally, for DCP_S, the rdf shows, like System CP_S, a first peak with maximum at 70 Å, but with a lower intensity, indicating a weaker dendrimer-dendrimer association. In addition a second broad peak is observed at around 140 Å, which nearly overlaps with that of DP_S. Representative snapshots of the systems with crowder in the presence of CTAB are presented in Fig. 4.6b-4.6d.

The middle row in Fig. 4.8 shows the rdfs between DNA and the different crowders, calculated based on the separation between DNA_{mon} and PEG_{mon}, $PMANa_{mon}$ or $PAMAM_{mon_5}$ (surface monomers). All distribution functions are very broad but some trends can, nevertheless, be seen. Considering the DNA and crowders alone (blue curves in middle row) it can be seen that, as expected, the neutral polymer is found, in average, closer to the DNA. There is however not a large accumulation of PEG monomers in the vicinity of the DNA as the maximum occurs at 90 Å, with $g(r)$ approximately 1.1 (Fig. 4.8d), that is, the systems are not very crowded. The depletion of the negatively charged crowders from the DNA vicinity is clear in Fig. 4.8e and 4.8f, with the spherical crowders showing a more defined peak than the linear one, which might be due to their larges charge density. Addition of CTAB to these systems leads to two different trends (pink curves). In Systems DCP_0 and DCP_S (panels d and f), the presence of CTAB leads to an increase in the average separation of DNA and crowders, as attested by the shift of

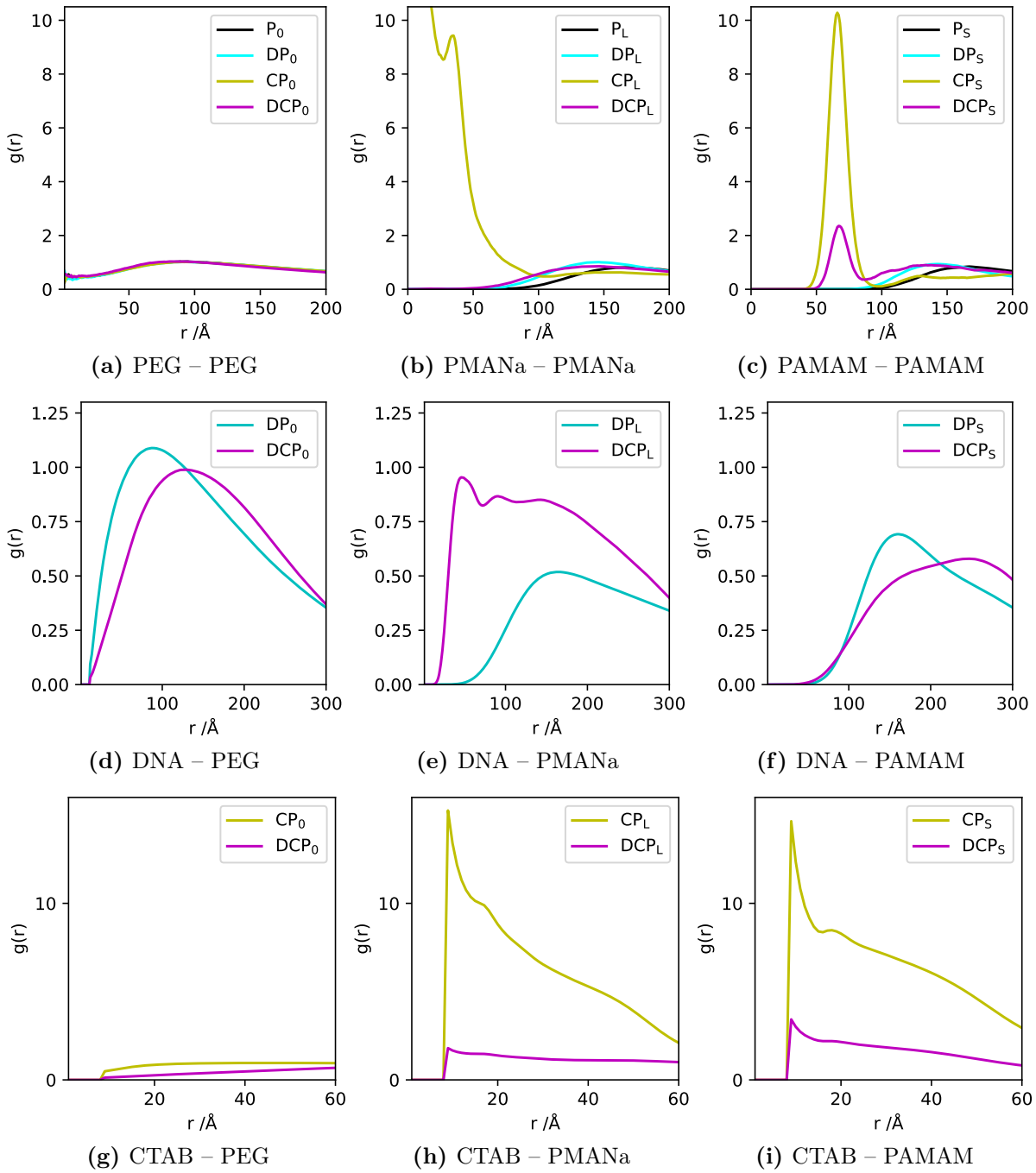

(a) PEG – PEG **(b)** PMANa – PMANa **(c)** PAMAM – PAMAM

(d) DNA – PEG **(e)** DNA – PMANa **(f)** DNA – PAMAM

(g) CTAB – PEG **(h)** CTAB – PMANa **(i)** CTAB – PAMAM

Figure 4.8: Radial distribution functions, $g(r)$, of (a) PEG – PEG, (b) PMANa – PMANa, (c) PAMAM – PAMAM, (d) DNA – PEG, (e) DNA – PMANa, (f) DNA – PAMAM, (g) CTAB – PEG, (h) CTAB – PMANa and (i) CTAB – PAMAM, for the systems indicated by the labels.

the peak towards longer distances, compared to the equivalent systems without CTAB. For the linear charged crowders, on the other hand, one observes a weak attraction (note the scale of the y-axis) between DNA and PMANa monomer, mediated by the CTAB.

Finally, the rdf of CTAB and crowder particle pairs are presented in the bottom row of Fig. 4.8, calculated based on the separation between $\mathrm{CTAB_{head}}$ and $\mathrm{PEG_{mon}}$, $\mathrm{PMANa_{mon}}$

or $PAMAM_{mon_5}$ (surface monomers). Fig. 4.8g shows the rdfs of CTAB – PEG. It can be seen that for the System CP_0 the components are roughly uniformly distributed in the simulation cell while the presence of DNA (System DCP_0) leads to some depletion of the CTAB from the vicinity of the PEG. The rdf of CTAB – PMANa, shown in Fig. 4.8h, shows for System CP_L a sharp increase at 8 Å, concomitant with the association of CTAB headgroups to the crowder. In the presence of DNA (System DCP_L, the peak at 8 Å is still present but with a much lower intensity, that is, the density of CTAB around the PMANa is much lower. The same trend is observed for CTAB – PAMAM pairs presented in Fig. 4.8i. However, when comparing to the linear crowder the intensity of the first peak seems to be lower in the absence of DNA but larger when DNA is present.

4.1.5 Conformation of crowders

The radius of gyration of PEG and PMANa are presented in Fig. 4.9a and 4.9b, respectively. The size distribution for PEG in System P_0 is centered around 45 Å, and does not change in the presence of DNA and/or CTAB. As expected, the $P(R_g)$ of PMANa in System P_L is shifted to larger sizes and centered around 60 Å. The chains have the same number of monomers, but the counterion release and charged monomers lead to the expansion of the chain. In System DP_L the distribution slightly broadens and shifts towards lower values. The size distribution in System CP_L shows a double maxima with one at 35 Å, and the second, with a lower intensity at around 60 Å. This suggests two populations of linear charged crowders, one corresponding to free chains and the other to PMANa – CTAB complexes, as shown in the snapshot of Fig. 4.6c. In System DCP_L the distribution is broader and shifted towards slightly lower values compared to System DP_L, that is, the presence of both DNA and CTAB does not seem to have a large effect on the conformation of PMANa. The size of PAMAM was assessed using the $g(r)$ of $PAMAM_{mon_1}$ – $PAMAM_{mon_5}$ pairs, and is shown in Fig. 4.9c. The size distribution in System P_S is centered around 25 Å. This result is only presented up to a radial distance where only one crowder is present, and is also only presented for System P_S, because the rdf cannot be employed to estimate the radius of the molecule if several crowders are closer than the presented range. One would also not expect the crowders to be significantly changed in other systems, because the model PAMAM is a hierarchical structure

of stiff chains.

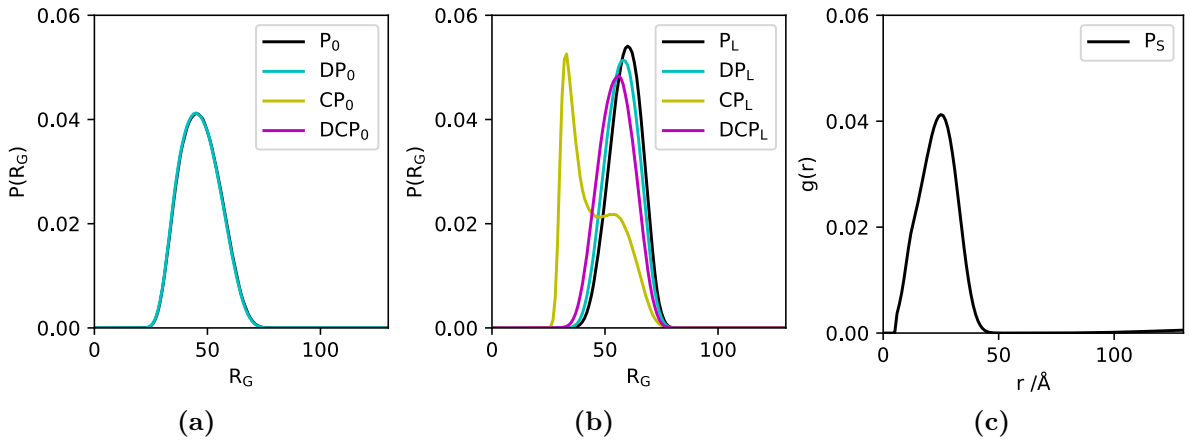

Figure 4.9: Probability distribution of the radius of gyration of (a) PEG and (b) PMANa, and (c) radial distribution function, $g(r)$, of $\text{PAMAM}_{\text{mon}_1}$ – $\text{PAMAM}_{\text{mon}_5}$ particle pairs, for the indicated systems.

4.2 Dye exclusion assay

The variation in fluorescence intensity due to the exclusion of a dye was used to monitor DNA availability to the dye in the presence of condensing and crowding molecules. All samples were prepared in triplicates and the results are presented as the mean including error bars based on the standard deviation.

4.2.1 Crowding effects

Results from DNA availability to GelStar in the presence of increasing concentrations of PEG in low salt concentrations are shown by the blue squares in Fig. 4.10a. The fluorescent intensity is measured at 535 nm and normalised to the control samples with DNA-GelStar alone. It can be seen that the fluorescent intensity increases almost linearly from 1 up to 1.6 when the concentration of PEG increases from 0 to 120 mg/mL. Above this concentration the intensity decreases and reaches a value of 1.25 at 180 mg/mL. Results from experiments conducted at high salt concentration ([NaBr] = 100 mM) are shown by the blue squares in Fig. 4.10b. The normalised intensity slowly increases from 1 up to 1.4 when the concentration of PEG increases from 0 to 60 mg/mL. From 60 to 120 mg/mL the intensity does not change significantly. Above PEG concentration of

120 mg/mL the intensity decreases rapidly from 1.4 to 0.5 at 180 mg/mL.

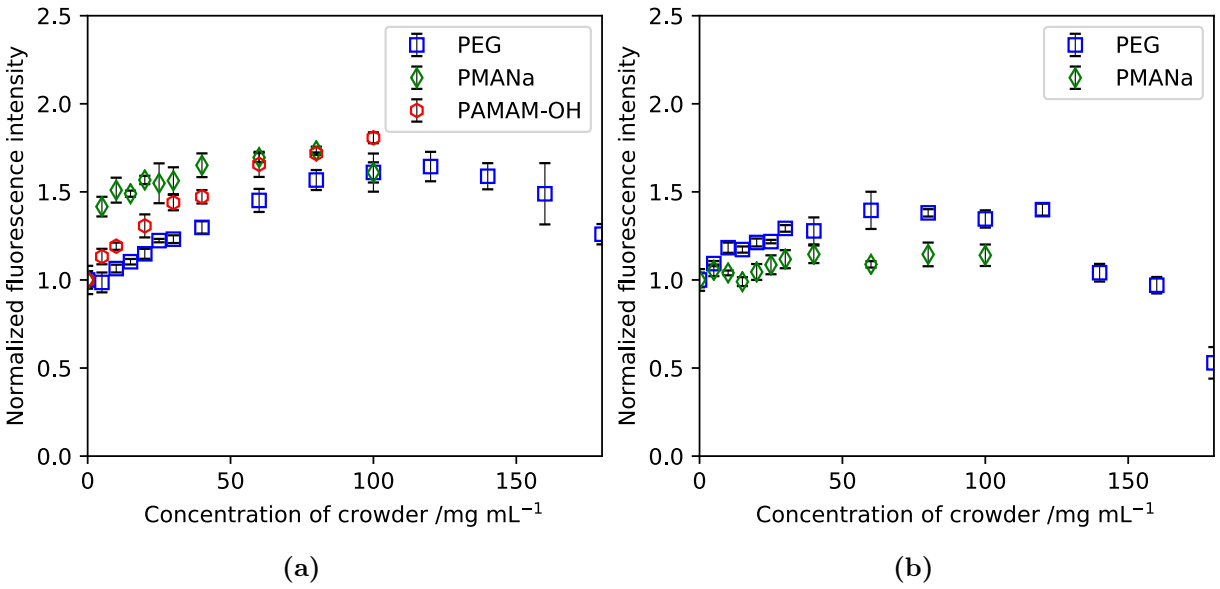

Figure 4.10: Fluorescent intensity from DNA-GelStar complex in (a) low salt concentration in the presence of increasing concentration of either PEG (blue squares), PMANa (green diamonds) or PAMAM-OH (red hexagons), or in (b) high salt concentration (100 mM NaBr) in the presence of increasing concentration of either PEG (blue squares) or PMANa (green diamonds). Fluorescent intensity is normalised with respect to samples containing DNA and GelStar. The results are based on triplicates and presented as mean with error bars indicating the standard deviation. Fluorescence was measured at 535 nm.

Results from dye exclusion from DNA in the presence of increasing concentration of PMANa are shown by the green diamonds in Fig. 4.10a. Increasing concentration of PMANa from 0 to 2.5 mg/mL results in a sharp increase in fluorescence intensity normalised to DNA-GelStar control from 1 to 1.4. Further increase of PMANa concentration to 80 mg/mL results in a steady increase in intensity to 1.7, however at 100 mg/mL the intensity is slightly reduced to 1.55. Results from similar experiments conducted at high salt concentration (green diamonds in Fig. 4.10b) show no significant changes in the fluorescence intensity in the range from 0 to 100 mg/mL PMANa.

Using PAMAM-OH as a crowding agent leads to the results shown by the red hexagons in Fig. 4.10a. Increasing the concentration of PAMAM-OH leads to a steady increase in fluorescence from 1 to 1.8 at 100 mg/mL PAMAM-OH.

4.2.2 Addition of surfactant with and without crowders

Fig. 4.11 shows the effect of CTAB addition to DNA in the presence and absence of different crowding agents. It gathers results obtained during the project assignment in the fall of 2019 and, thus, not part of the work performed in this thesis, for completeness. These are identified in the text and figure caption. The fluorescent intensity is measured at 535 nm and normalised to the control samples with DNA-GelStar alone. Samples in the presence of increasing concentration of CTAB and no crowders, are shown by the black circles. The results show a rapid decrease in fluorescence from 1 at 0 μM CTAB to 0.2 at 25 μM. Further increase of CTAB above 25 μM CTAB does not cause a change in the fluorescence intensity.

The effect of adding 25 mg/mL PEG to the DNA-CTAB series is shown by the blue squares. At 0 μM CTAB, the addition of PEG does not significantly change the intensity compared to its absence. Increasing the concentration of CTAB leads to a decrease in intensity which stabilises at a value of 0.5 in the range 10 to 15 μM CTAB. Further increase of CTAB results in a decrease in intensity and above 30 μM the intensity does not change significantly and has a value of approximately 0.2.

Two different concentrations were tested for PMANa crowders. The results obtained for DNA in the presence of 13 mg/mL PMANa and increasing concentration of CTAB are shown by the cyan triangles in Fig. 4.11. In the absence of CTAB, the addition of PMANa leads to an increase in intensity from 1.0 to 1.4. Increasing the concentration of CTAB up to 300 μM (only up to 50 μM is presented) did not change the intensity significantly. Increasing the PMANa concentration to 25 mg/mL (green diamonds in Fig. 4.11) leads to similar variations in the normalised intensity. Without CTAB the intensity increases from 1.0 (absence of crowder) to 1.6. Increasing the CTAB concentration to 300 μM (only up to 50 μM is presented) does not significantly change the intensity.

Two different concentrations were tested for the PAMAM-OH crowders. During the project assignment 15 mg/mL PAMAM-OH was used (purple triangles in Fig. 4.11). The addition of 15 mg/mL PAMAM-OH leads to an increase in the normalised intensity to 1.5 at 0 μM CTAB, compared to the intensity of 1 in the absence of PAMAM-OH. Increasing the concentration of CTAB to 5 μM leads to a significant drop in the intensity to 1.25 followed by a plateau up to a CTAB concentration of 20 μM. When the concentration

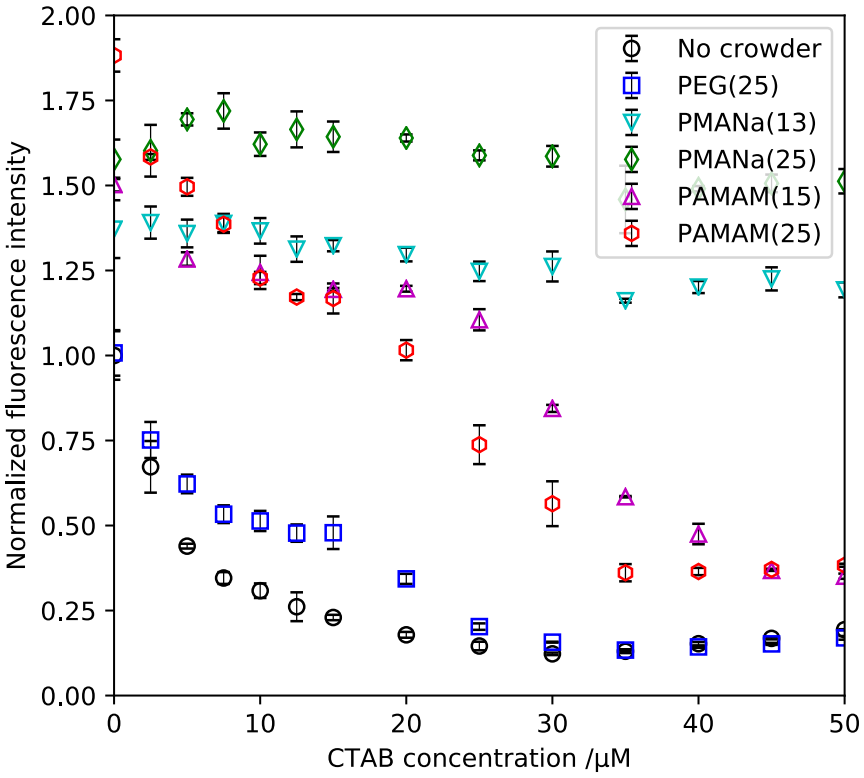

Figure 4.11: Normalised fluorescence intensity from DNA-GelStar complex in the absence of crowder (black circles) and in the presence of either 25 mg/mL PEG (blue squares), 13 mg/mL PMANa (cyan triangles), 25 mg/mL PMANa (green diamonds), 15 mg/mL PAMAM-OH (purple triangles) or 25 mg/mL PAMAM-OH (red hexagons), as a function of increasing concentration of CTAB. The fluorescence was measured at 535 nm and normalised to samples with DNA and GelStar. The results are based on triplicates and presented as mean with error bars, indicating the standard deviation. Results shown by the black and purple circles were obtained during the project assignment in the fall of 2019.

of CTAB exceeds 25 μM the intensity starts decreasing and reaches a stable value of 0.4 above 45 μM. Increasing the PAMAM-OH concentration to 25 mg/mL (red hexagons in Fig. 4.11) leads to similar variations in the normalised intensity. At 0 μM CTAB the fluorescent intensity is almost double compared to samples without PAMAM-OH, which is much larger than the normalised fluorescence at 25 mg/mL PAMAM-OH in Fig. 4.10a. Increasing the concentration of CTAB to 10 μM leads to a decrease in intensity to 1.25. In the range 10 to 15 μM CTAB the intensity does not change significantly. Further increase of CTAB leads to a new decrease in intensity, and above 35 μM CTAB the intensity stabilises at an intensity of 0.4.

The addition of 100 mM NaBr to the DNA-CTAB systems, in the presence and absence of crowders, leads to significant changes, as seen in Fig. 4.12. The fluorescence

is again measured at 535 nm and normalised to samples with DNA-GelStar in 100 mM NaBr, which in turn has a fluorescence of 1.2 compared to DNA-GelStar in the absence of salt. The black circles shown the results obtained in the absence of crowders. Increasing the concentration of CTAB from 0 to 7.5 µM leads to a decrease in the normalised fluorescence intensity to 0.8. Above this concentration and up to 20 µM the intensity does not change. Further increase of the concentration results in a decrease in intensity, and above 45 µM CTAB the intensity has stabilised at an intensity of 0.2.

The addition of PEG is shown by the blue squares in Fig. 4.12. At 0 µM CTAB, the

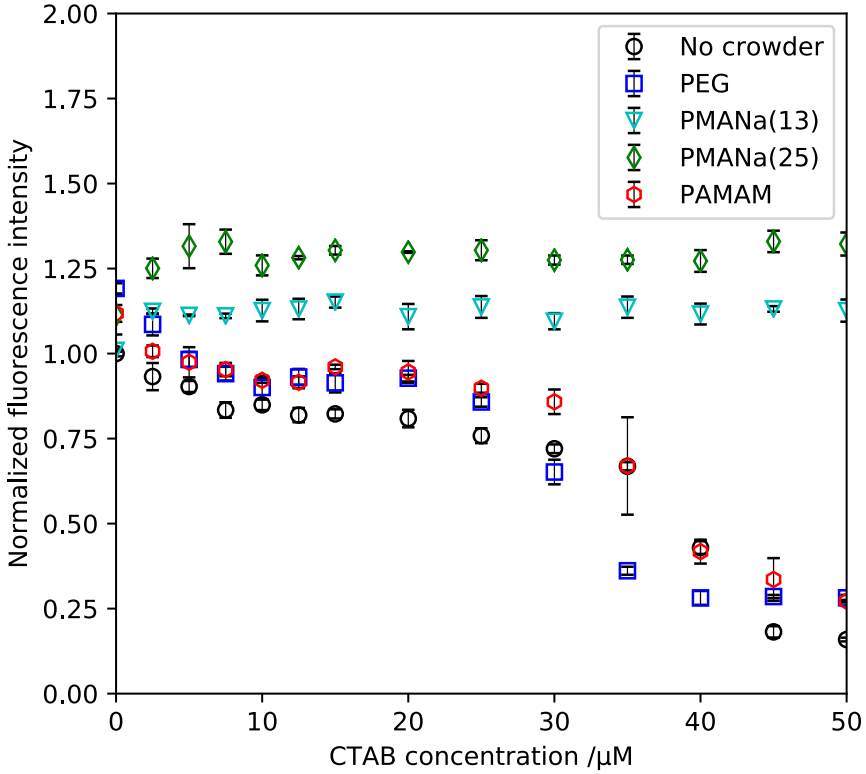

Figure 4.12: Normalised fluorescent intensity from DNA-GelStar complex in 100 mM NaBr in the absence of crowder (black circles) and in the presence of either 25 mg/mL PEG (blue squares), 13 mg/mL PMANa (cyan triangles), 25 mg/mL PMANa (green diamonds) or 25 mg/mL PAMAM-OH (red hexagons) as a function of increasing concentration of CTAB. The fluorescence was measured at 535 nm and normalised to samples with DNA and GelStar in 100 mM NaBr. Results are based on triplicates and presented as mean with error bars, indicating the standard deviation.

addition of 25 mg/mL PEG leads to a slight increase in intensity from 1 to 1.2. Increasing the concentration of CTAB reduces the fluorescence intensity, which stabilises at a value of 0.9 in the range 10 to 20 µM CTAB. Above this concentration the intensity drops quite

rapidly to 0.25 and does not change significantly above 40 μM.

Replacing the PEG with 13 mg/mL or 25 mg/mL PMANa again leads to a different trend (cyan triangles and green diamonds in Fig. 4.12). An increase from 1 to 1.1 is observed when increasing the CTAB concentration to 2.5 μM in the presence of 13 mg/mL PMANa, but further increase to 300 μM CTAB (only up to 50 μM is presented). At 0 μM CTAB the intensity increases from 1 to 1.1 upon addition of 25 mg/mL PMANa. Increasing the concentration of CTAB to 2.5 μM induces a slight increase in intensity to 1.25, and above this concentration the intensity does not change significantly.

Using PAMAM-OH as crowder is show as red hexagons in Fig. 4.12. Addition of 25 mg/mL PAMAM-OH shows a slight increase in intensity from 1 to 1.1 at 0 μM CTAB. Increasing the concentration of CTAB to 7.5 μM slightly lowers the intensity to 0.9. Further increase of CTAB up to 20 μM does not change the intensity significantly. At 25 and 30 μM the intensity slightly drops, however further increase of CTAB to 50 μM results in a significant drop in the intensity to 0.25.

The results of the diverse control samples that were performed are shown in Table 4.1. As before, fluorescence intensity was measured at 535 nm and normalised to the intensity from DNA-Gelstar complex at 535 nm. The normalised intensity from GelStar is 27.7×10^{-3}, and addition of 25 mg/mL PEG, 25 mg/mL PMANa or 25 mg/mL PAMAM increases the intensity to 51.2×10^{-3}, 34.5×10^{-3} and 132.1×10^{-3}, respectively. Addition of NaBr decreases the intensity in the absence and presence of crowders. Addition of CTAB increases the intensity to 39.3×10^{-3}, 60.0×10^{-3}, 75.2×10^{-3} and 180.0×10^{-3} for no crowder, PEG, PMANa and PAMAM, respectively. Addition of both CTAB and NaBr decreases the intensity, compared to in the absence of NaBr, to 36.7×10^{-3}, 55.4×10^{-3}, 69.5×10^{-3} and 124.1×10^{-3}, respectively.

4.3 Electrophoretic mobility shift assay

Electrophoretic mobility shift assays were performed to assess the effect of different crowders on the mobility of DNA+CTAB complexes in two different salt concentrations. The top panel in Fig. 4.13 shows the effect of crowding induced by PEG under low salt concentration. Lane 1 shows free DNA, lanes 2 to 8 show DNA with increasing concentration of CTAB, lane 9 shows DNA with crowder (25 mg/mL PEG) and lanes 10-16 refer to DNA

Table 4.1: Fluorescence intensity of Gelstar in the absence and presence of CTAB (50 μM), NaBr (100 mM) or both (column 2), and GelStar with 25 mg/mL PEG in the absence and presence of CTAB, NaBr or both (column 3), 25 mg/mL PMANa in the absence and presence of CTAB, NaBr or both (column 4) and 25 mg/mL PAMAM-OH in the absence and presence of CTAB, NaBr or both (column 5), normalised to samples with DNA and GelStar (I/I_0). Excitation wavelength was 493 nm, and emission was measured at 535 nm. The values are based on triplicated and presented as mean with standard deviation.

	No crowder $/10^{-3}$	PEG $/10^{-3}$	PMANa $/10^{-3}$	PAMAM $/10^{-3}$
-	27.7 ± 0.7	51.2 ± 1.0	34.5 ± 0.5	132.1 ± 7.0
NaBr	19.3 ± 0.7	45.8 ± 0.7	25.3 ± 0.4	80.8 ± 2.7
CTAB	39.3 ± 0.2	60.0 ± 0.8	75.2 ± 1.2	180.0 ± 1.1
CTAB+NaBr	36.7 ± 0.1	55.4 ± 2.8	69.5 ± 1.3	124.1 ± 2.5

with crowder and increasing concentration of CTAB. It can be seen that in the absence of PEG, the addition of up to 50 μM CTAB does not change the shape of the bands significantly. From 100 to 300 μM the bands become more smeared out for each step, indicating the formation of DNA-CTAB aggregates with a wide distribution of sizes and/or charge. At 500-800 μM, the bands are still smeared, however the bands have shifted to lower ranges, that is, the complexes have migrated less. The effect of adding PEG is shown by the 8 lanes to the right. The addition of PEG to DNA (lane 9) shows no significant effect compared to lane 1, with DNA only, as well as the addition of 10 and 50 μM CTAB. At 100 μM the band is significantly smeared in comparison with lane 4. Increasing the CTAB concentration leads to a broadening of the band, but up to 300 μM CTAB there is still indications of intensity at longer ranges. At 500 μM the band indicates a lack of naked DNA or very charged complexes, and at 800 μM the sample has almost zero range through the gel. Comparing the sample set with and without PEG, it can be seen that the presence of PEG enhances the DNA condensation by CTAB.

The middle panel in Fig. 4.13 gathers the results of using PMANa as a crowding agent in low salt concentration. Lanes 1 to 8 show control samples with increasing CTAB and absence of PMANa, and show similar trends as the equivalent samples in lanes 1-8 in the top panel in Fig. 4.13, with an increased band broadening from 100 μM CTAB. However, the samples at larger CTAB concentrations (500 and 800 μM) do not seem to present the same level of condensation, which is unexpected. With PMANa, some band broadening is observed at higher CTAB concentrations, 200 and 300 μM. The intensity of the band at 200 μM is much higher compared to the others. At 500 and 800 μM CTAB

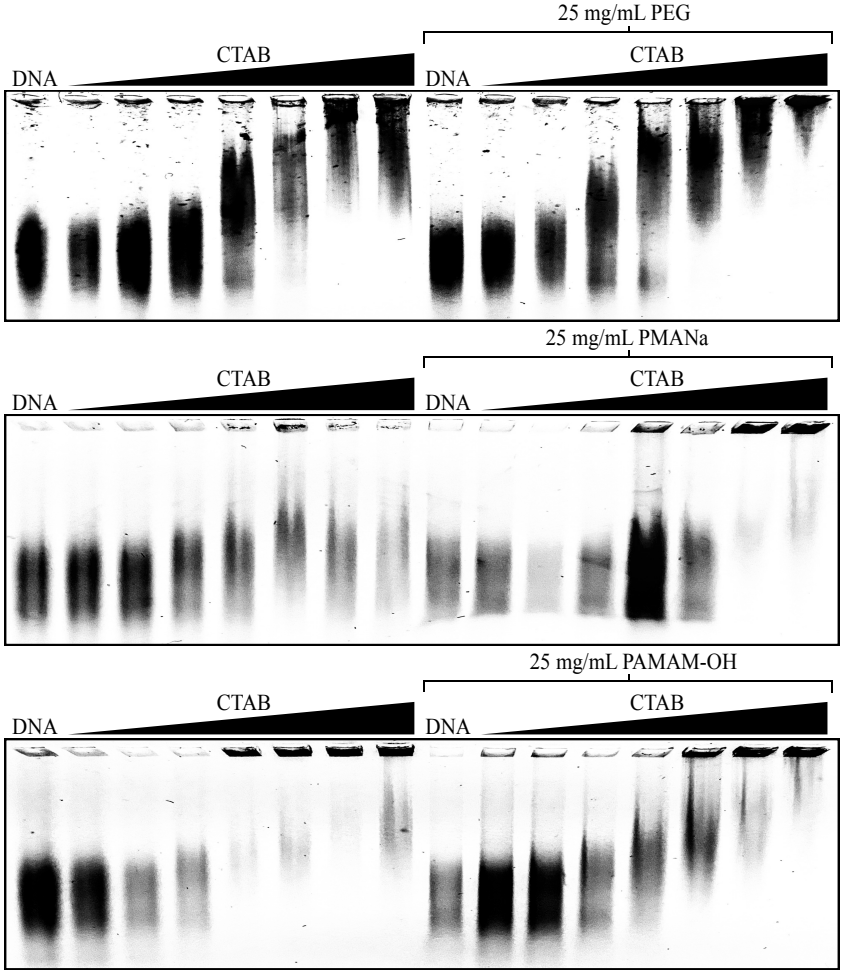

Figure 4.13: Electrophoretic mobility shift assay of 25 μg/mL DNA with increasing CTAB concentration (0, 10, 50, 100, 200, 300, 500, 800 μM) in the absence (lanes 1-8) and presence (lanes 9-16) of 25 mg/mL PEG (top panel), 25 mg/mL PMANa (middle panel) or 25 mg/mL PAMAM-OH (bottom panel).

the majority of the DNA is found in the wells.

The results from EMSA on DNA-CTAB complexes with PAMAM-OH is presented in the bottom panel in Fig. 4.13. Although the intensity in this gel is lower, the results of the DNA-CTAB samples (lanes 1-8) are consistent with those described above (e.g. lanes 1-8 in the top and middle panel in Fig. 4.13). Addition of PAMAM-OH leads to a broadening of the band at 100 μM. At 200 μM the band has a similar width as at 100 μM, however the band is shifted closer to the well. As the concentration of CTAB increases above 200 μM the bands shifts closer to the well and the intensity observed in the wells increases, and at the highest CTAB concentration more of the sample is contained within the well, compared to in the absence of crowder.

EMSA of DNA in 100 mM NaBr with PEG and increasing concentration of CTAB is shown in Fig. 4.14. Without PEG (lanes 1-8 in all three gels), the broadening of the bands is noticeable at 100 μM CTAB. As the concentration of CTAB increases, the bands are further shifted toward the wells and the intensity in the wells increases. With PEG, the broadening of the band occurs at 100 μM and is intensified with the addition of 200 and 300 μM CTAB. At 500 μM the band is shifted towards the well, with an increase in fluorescence intensity in the well. At 800 μM most intensity is visible in the well, indicating that the DNA is neutralised and/or the DNA-CTAB complexes are too large to penetrate the gel.

EMSA of DNA-CTAB complexes with PMANa in high salt concentration is pre-

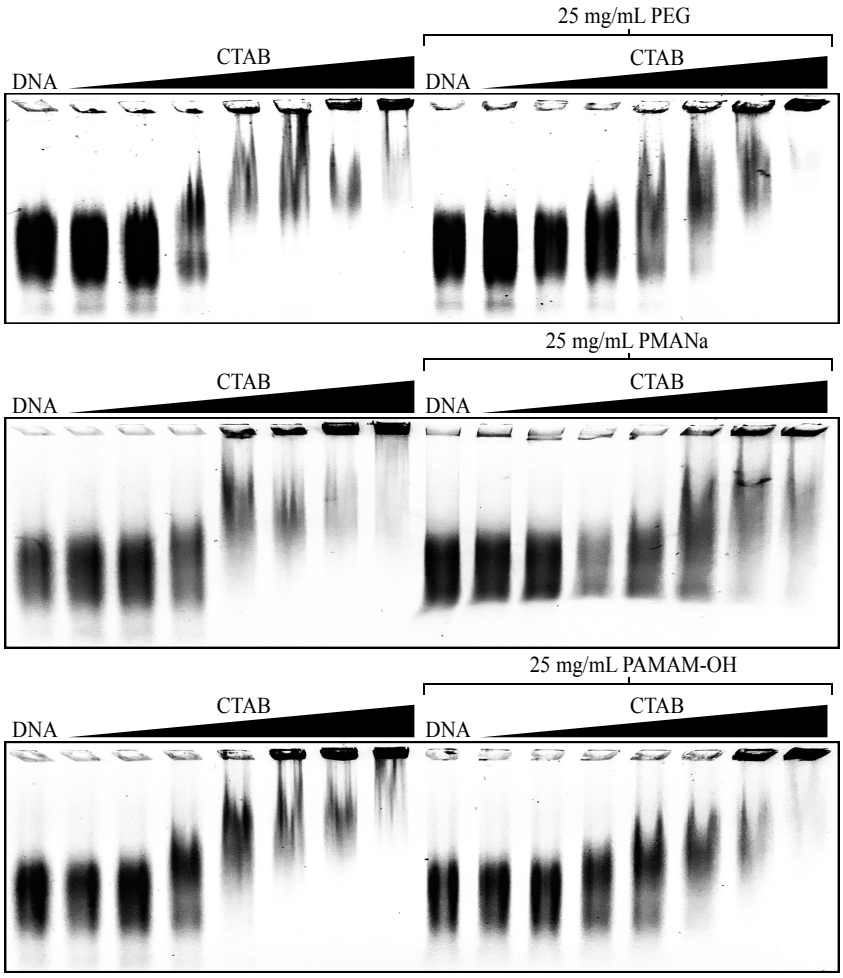

Figure 4.14: Electrophoretic mobility shift assay of 25 μg/mL DNA (in 100 mM NaBr) with increasing CTAB concentration (0, 10, 50, 100, 200, 300, 500, 800 μM) in the absence (lanes 1-8) and presence (lanes 9-16) of 25 mg/mL PEG (top panel), 25 mg/mL PMANa (middle panel) or 25 mg/mL PAMAM-OH (bottom panel).

sented in the middle panel in Fig, 4.14. It can be seen that in the presence of PMANa, the band broadening only occurs at 200 μM. Above this CTAB concentration the bands shift slightly towards the wells, however some intensity is still visible at ranges similar to 0 μM CTAB, indicating the presence of free DNA. Some DNA seems to be present in the wells at 300 μM, and this is more prominent at 500 and 800 μM CTAB.

EMSA of DNA in the presence of CTAB and PAMAM-OH in high salt concentration is presented in the bottom panel in Fig. 4.14. With PAMAM-OH, broadening of the band also occurs at 100 μM (as observed in control samples), but to a lesser degree, and this effect gets more prominent as the concentration increases to 300 μM. Only at 500 μM CTAB is the band shifted closer to the well and the DNA-CTAB complexes found in the well. At 800 μM the band is shifted even closer to the well and the intensity from the well does increases even more.

To summarize, PEG is found to enhance DNA condensation by CTAB, while the negatively charged polyions reduce the condensation, independently of the salt concentration. PAMAM-OH appears to affect the DNA-CTAB complexes less, when compared to PMANa.

4.4 DNase protection assay

Here the results from DNase protection assay in the presence of crowders are presented. In the following figures, lane 1 shows free DNA, lane 2 shows DNA digested with DNase I for 30 minutes, lanes 3 to 8 show DNA in the presence of increasing concentration of CTAB, and digested with DNase. Lane 9, similarly to lane 1, shows free DNA, lane 10 shows DNA in the presence of 25 mg/mL crowder and digested with DNase I, and lanes 11-16 show DNA in the presence of 25 mg/mL crowder, increasing concentration of CTAB and digested with DNase I.

Fig. 4.15 shows how the increasing concentration of CTAB in the absence and presence of crowders affect digestion of DNA by DNase at low salt concentration. The first 8 lanes in all gels show the control samples performed in the absence of crowders. All gels show similar results, showing the consistency of this methodology. Starting with lane 2, showing the results of DNA digestion by DNase for 30 minutes, it can be seen that the DNA is shifted away from the well, in comparison with the undigested DNA (lane

1), indicating that the DNA molecules are shorter. The addition of 50 μM CTAB to the sample prior to digestion by DNase leads to a band that is similar to that of lane 1, albeit with a lower intensity. A slight increase in intensity is also observed in the well, indicating digested DNA molecules neutralised by the interaction with CTAB. From 100 μM CTAB the bands become weaker and shift towards the wells. The intensity in the wells also increases.

Results from the DNase protection assay using PEG as a crowding agent are presented in the top panel in Fig. 4.15. Lanes 10-16 show the results obtained upon addition of PEG prior to DNA digestion by DNase. Although the bands have a low intensity, it can be seen that the PEG does not prevent the digestion of DNA by DNase, with a band appearing at sizes equivalent to those of lane 2 (DNA digested without PEG), and smaller than those of lane 9 (DNA control). Addition of 50 μM CTAB leads to the broadening of the band such that is appears to include sizes of bands 9 and 10. Above this concentration the bands become broader compared to lane 9, and shift closer to the wells as CTAB increases. The intensity from the wells also increases significantly.

Results from DNase protection assay using PMANa are presented in the middle panel in Fig. 4.15. Lane 9 with a similar sample as lane 1, has a distortion where the band is smeared to the left. With PMANa all the bands stop at a range similar to that of the center of the band in lanes 1 and 9. At 0 μM CTAB the intensity of the band is very low, with 50 μM CTAB the intensity is higher, and it decreases again for 100 μM. At 200 μM CTAB the band is broadened, and this effect is even more noticeable at 300 μM CTAB. At these concentrations there is a slight increase in the intensity in the wells. At 500 μM the intensity from the band decreases and the intensity in the well increases. At 800 μM the band intensity is very low and the intensity from the well has decreased compared to 500 μM CTAB.

Results from DNase protection assay using PAMAM-OH dendrimers are presented in the bottom panel in Fig. 4.15. In the presence of PAMAM-OH the band displays a similar broadening as in the absence of crowder, with two maxima in the intensity, indicating free and digested DNA. Upon addition of 50 μM CTAB, prior to digestion, the band broadens, shifts to a similar range of free DNA and the intensity in the well increases. An increase in CTAB concentration to 100 μM leads to a shift of the band towards the

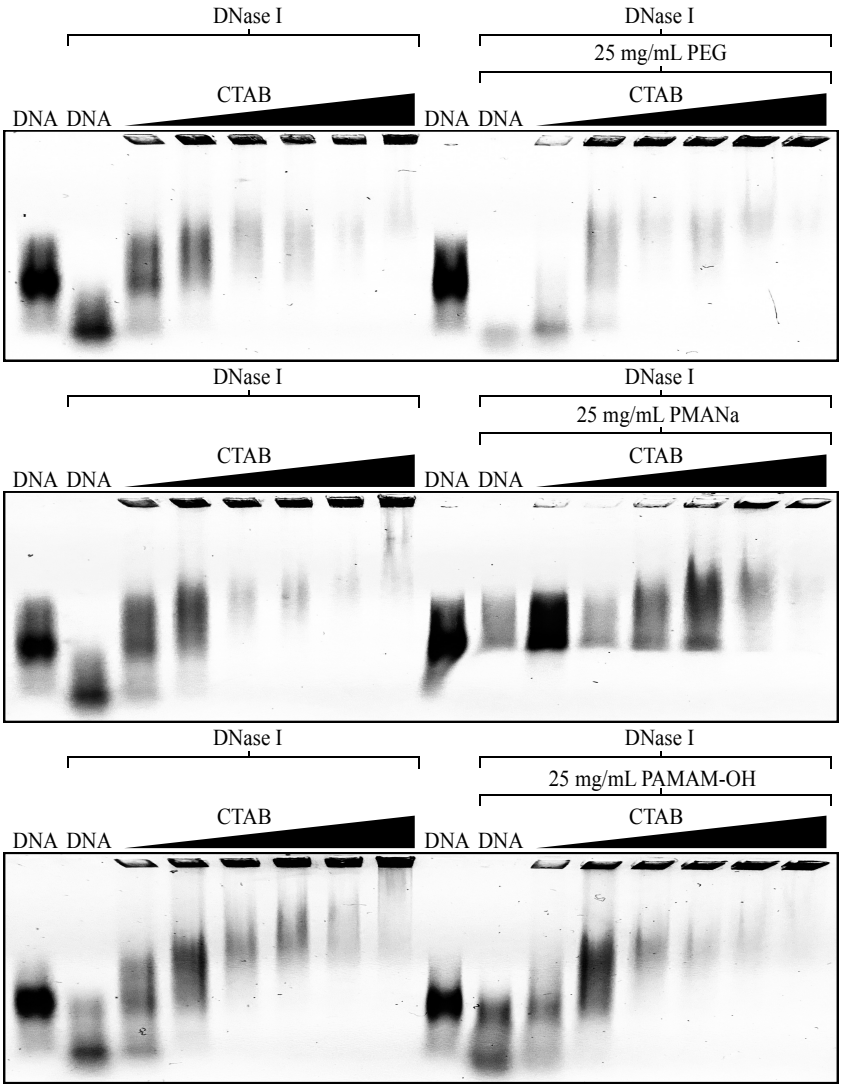

Figure 4.15: DNase protection assay of 25 μg/mL DNA with increasing CTAB concentration (0, 50, 100, 200, 300, 500, 800 μM) in the absence (lanes 2-8) and presence (lanes 10-16) of 25 mg/mL PEG (top panel), 25 mg/mL PMANa (middle panel) or 25 mg/mL PAMAM-OH (bottom panel). Lanes 1 and 9 show free DNA.

well, an increase in intensity, and an increase in intensity from the well. Increasing the concentration of CTAB to 200 μM, the band gets shorter, it is shifted towards the well, the intensity decreases, and the intensity form the well increases. At the highest studied CTAB concentration (800 μM) almost only the intensity in the well is visible.

Fig. 4.16 shows the DNase digestion studies performed for DNA-CTAB samples in the presence and absence of the diverse crowder molecules at high salt concentration. The first 8 lanes in all gels show the control samples performed by the digestion of DNA-CTAB complexes at high salt concentration. It can be seen that, compared with the systems

with less salt, the intensity of the bands is higher and the DNA digestion less efficient as noticed by the small shift of the band in lane 2 compared to lane 1 (i.e. digested vs. non-digested DNA). Addition of CTAB (50 μM) to the samples prior to digestion leads to the protection of most DNA, as seen by the shifts towards larger sizes; also a slight intensity is noticeable in the well. As the concentration of CTAB increases the bands shifts closer to the well, the intensity from the band decreases and the intensity from the wells increases. At 800 μM the band is barely visible, indicating almost all DNA-CTAB complexes are neutralised and/or too large to migrate from the well.

The addition of crowders lead to some variation in the described behaviour. The addition of PEG seems to enhance DNA digested (lane 10 versus lane 2). Addition of 50 μM CTAB does not seem to affect the shape of the band, but its intensity decreases significantly. Increasing the CTAB concentration further leads to the almost disappearance of the DNA bands from the gel (with exception of 100 μM) and an increase in the fluorescence intensity in the wells.

Results from DNase protection assay using PMANa as crowding agent are shown in the middle panel in Fig. 4.16. The addition of PMANa clearly affects the mobility of DNA through the gel, which was also observed in low salt concentration (middle panel in Fig. 4.15). The addition of PMANa enhances DNA digestion as shown by the very low intensity in the band in lane 10 compared to lane 2. Addition of CTAB (50 μM) further enhances digestion of DNA, however at 100 μM the intensity of the band is higher compared to 50 μM, indicating more protection of DNA. Further increase in CTAB concentration leads to a broadening of the band and an increase in fluorescence intensity in the wells. At 500 and 800 μM CTAB the bands are nearly visible.

Results from DNase protection assay using PAMAM-OH in high salt concentration are presented in the bottom panel in Fig. 4.16. Using PAMAM-OH the DNA band appears more broadened and shifted further away from the well at both 0 and 50 μM CTAB, compared to the in the absence of crowder. A slight intensity is visible in the well at 50 μM. At 100 μM the band becomes broader and is shifted towards the well, and the intensity in the well is higher. As CTAB increases the bands shift closer to the wells, their intensity decreases and the intensity in the wells increases.

To summarize, it was observed that at concentration of CTAB of 50 μM and above,

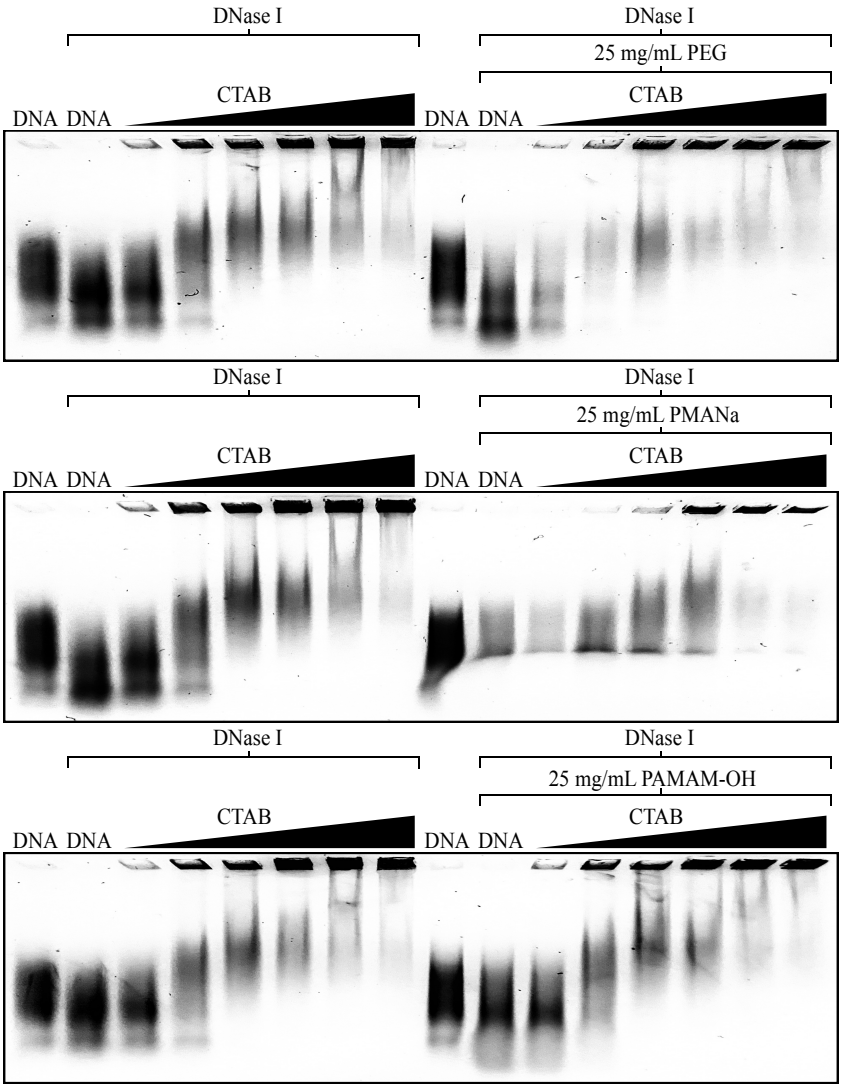

Figure 4.16: DNase protection assay of 25 µg/mL DNA (in 100 mM NaBr) with increasing CTAB concentration (0, 50, 100, 200, 300, 500, 800 µM) in the absence (lanes 2-8) and presence (lanes 10-16) of 25 mg/mL PEG (top panel), 25 mg/mL PMANa (middle panel) or 25 mg/mL PAMAM-OH (bottom panel). Lanes 1 and 9 show free DNA.

the surfactant is able to protect the DNA from DNase digestion, at least to some extent. The addition of PEG leads to an increase in the digestion at low CTAB concentration. A higher CTAB concentrations the bands are visible in the gel, which could be due to the improved DNA condensation by CTAB and PEG (see top panel in Fig. 4.13). With PAMAM-OH, the results are very similar, with the exception of the more intense bands at low CTAB concentrations. The PMANa, on the other hand shows very little variation in the band with increasing CTAB concentration. Increasing the salt concentration leads to a weaker digestion of DNA by DNase and the described overall trends for low salt concentration are kept for all crowders.

Chapter 5

Discussion

Aiming at further highlighting on the effect of macromolecular crowders on DNA condensation induced by CTAB, Monte Carlo simulations and experimental work has been performed. In the following sections the results from Monte Carlo simulation and *in vitro* studies at low and high ionic strength are discussed.

5.1 DNA condensation by CTAB

In this work the cationic surfactant CTAB is used to mimic self-associating proteins. DNA condensation induced by cationic surfactants has been subject of many studies [56]. As mentioned in the introduction, at a generally well-defined concentration, the critical micellar concentration (CMC), surfactants form aggregates in solution. If the surfactants are charged the presence of an oppositely charged macromolecule, e.g. DNA, leads to their aggregation in the vicinity of the macromolecule at the so-called critical association concentration (CAC).

5.1.1 Experimental approach

The CAC of CTAB with 100 μM DNA in 2 mM Tris-HCl buffer pH 7.6 has been estimated to be 4 ± 1 μM [57]. It has been shown that the CAC is nearly independent on DNA concentration, which should allow for a direct comparison to the results obtained here. However, as seen by the results from dye exclusion assay (black circles in Fig. 4.11) the fluorescence decreases significantly by adding 2.5 μM CTAB, which indicates that DNA starts condensing at this concentration under the conditions used in this work. Other authors have shown that DNA starts to transition from coil to globule at 9.5 μM CTAB

and reaches a condensed state at around 20 μM [58], and another study has shown that DNA starts condensing at a CTAB/DNA charge ratio $r_{charge} = 3$, but required $r_{charge} = 6$ to fully condense DNA [59]. In this work the charge ratio of CTAB/DNA equals 0.4 at 2.5 μM CTAB and a ratio of 5.7 is required to fully condense DNA. Thus, DNA was found to start condensation at a lower CTAB concentration than expected, however, the DNA is fully condensed at a similar concentration and charge ratio as has previously been observed.

EMSA was also used to investigate DNA condensation. Seeing as the CAC of CTAB has been reported to not change significantly with the concentration of DNA, one would expect CTAB to start associating with the polyelectrolyte at a similar concentration. The mobility of DNA and visibility of the DNA bands is somewhat dependent on gel preparation, therefore, DNA in the presence of increasing concentration of CTAB is used as reference samples in all EMSA studies. The three results from EMSA (lanes 1-8 in all panels in Fig. 4.13) indicates that a concentration of 100 μM is required to affect the mobility of DNA. In the dye exclusion assays a charge ratio of 0.4 was enough to lower the fluorescence intensity, however in EMSA the charge ratio at 50 and 100 μM equals 0.65 and 1.3, respectively, which indicates that a higher CTAB to DNA charge ratio is required to observe DNA condensation using EMSA. During the electrophoresis, DNA and CTAB are pulled in opposite directions in the gel, i.e. towards the anode and cathode, respectively. It has previously been discussed that the electric field may greatly affect the condensation process, where a large difference in condensation threshold was observed when comparing experiments conducted at high and low voltage [60]. EMSA is therefore not the best approach to study DNA condensation. However, since the changes to the offset of condensation caused by the electric field will be the same for all samples, the technique can be used to investigate the effect of crowder addition to DNA-CTAB samples. Nevertheless it could explain why a higher CTAB to DNA charge ratio is needed to induce DNA condensation. Also, it is difficult to know if the effect observed at charge ratio 0.4 in the dye exclusion assays would have affected the mobility of DNA in EMSA.

The assessment of the CTAB concentration that leads to a complete DNA condensation is more challenging. The band for [CTAB] = 800 μM, in the top panel in Fig. 4.13, indicates that a large fraction of DNA is condensed, however in the middle panel none

seems to be condensed, and in the bottom panel almost all DNA is condensed, taking into account the large intensity at the well and lack of band. This exemplifies the variation often observed in these experiments.

DNase protection assay was used to investigate the protection granted by CTAB towards the enzymatic activity of DNase I. It can be seen in the lanes 1-8 of all panels in Fig. 4.15 that the addition of 50 μM is enough to prevent significant digestion of the DNA, as seen by the lack of bands with sizes smaller than that of the undigested DNA (lane 1). This is consistent with results from EMSA, where formation of larger and/neutral DNA-CTAB complexes was observed at 100 μM CTAB. Furthermore, the appearance of fluorescence intensity in the wells, indicating neutralised DNA or large DNA-CTAB complexes, occur at lower CTAB concentrations than the samples that were not digested (see Fig. 4.13). DNase I cleaves DNA in a statistical manner, which allows for the presence and condensation of shorter DNA molecules at lower CTAB concentrations.

5.1.2 Modeling approach

Monte Carlo simulations were performed, where analysis of the radius of gyration of a model DNA, cluster formation of CTAB and interaction between DNA-CTAB were evaluated. Since the used model describes the solvent as a continuum, the hydrophobic effect was modeled by a Lennard-Jones potential (Eq. 2.4). The strength of the attractive potential between CTAB molecules, ϵ, was chosen such that the CTAB self-assembled in the presence of DNA. Results from equilibrium runs (not presented) showed that $\epsilon = 2$ kT and $N_{\mathrm{CTAB}} = 960$ or $N_{\mathrm{CTAB}} = 1440$, did not induce the self-assembly of CTAB. However, using $\epsilon = 3$ kT and $N_{\mathrm{CTAB}} = 960$ did.

It was interesting to see that the model CTAB did not self-assemble in the absence of DNA (System C) (Fig. 4.6a), which is evident from the rdf of CTAB – CTAB (Fig. 4.5a) and cluster size analysis (Fig. 4.7a), which indicates that the concentration of CTAB in this model system is below the CMC.

When adding DNA, the self-assembly of CTAB will occur in the vicinity of DNA due to the release of counterions and consequent electrostatic interactions between the negatively charged polyelectrolyte and the positively charged surfactant headgroups. The CTAB

molecules form spherical/ellipsoid aggregate with the positively charged headgroups facing outwards which interacts with the monomers of the polyelectrolyte. This induces the wrapping of the DNA (see Fig. 4.2e), which greatly affects its conformation as seen by the significant shift of the size distribution, $P(R_G)$, towards lower values (filled vs dashed black curves in Fig. 4.1). There is a large number of CTAB headgroups in contact with each DNA monomer (Fig. 4.4a), and its wrapping around the CTAB micelles is clearly visible by the maxima and minima in the contact analyses, which also indicates that several monomers are in contact with multiple CTAB micelles. Previous work has shown that the aggregation number of CTAB is approximately 70 when the concentration of CTAB is 5-50 times the CMC [61, 62]. This aggregation number coincides quite well with the results obtained here. However, the reported number refers to CTAB aggregated in the absence of DNA, and its presence is likely to increase the aggregation number of CTAB, due to the decrease in electrostatic repulsion between the headgroups and an increase in the critical packing parameter.

5.2 Effect of crowder molecules on DNA-CTAB interaction

In the presence of a large concentration of macromolecules, macromolecular crowding is expected to influence the interaction of DNA with CTAB. In this work different types of crowders were used, a neutral linear polymer, and linear and spherical-like negatively charged polymers. Due to material limitations and the long computational times, the concentration of crowder molecules in the experiments was not enough to induce molecular crowding. It was however possible to assess the impact of the various crowder molecules.

The fluorescence measurements presented in Fig. 4.11, show a large increase in fluorescence intensity upon the addition of the negative crowders to the DNA + GelStar systems. It is unclear why this happens, since the crowder do not seem to affect the fluorescence of GelStar to such a large degree on their own (see Table 4.1). Since the presence of the diverse components seems to increase the intensity, it is assumed that a decrease in intensity is related to the exclusion of the GelStar from the DNA due to its condensation. To better assess the differences between the crowders, the results from dye

exclusion assays in Fig. 4.11 (normalized to the DNA+GelStar control samples) were re-plotted by normalizing each sample set to the respective DNA+GelStar+crowder controls instead. That is, all series have $I/I_0 = 1$ at 0 µM CTAB (Fig. 5.1).

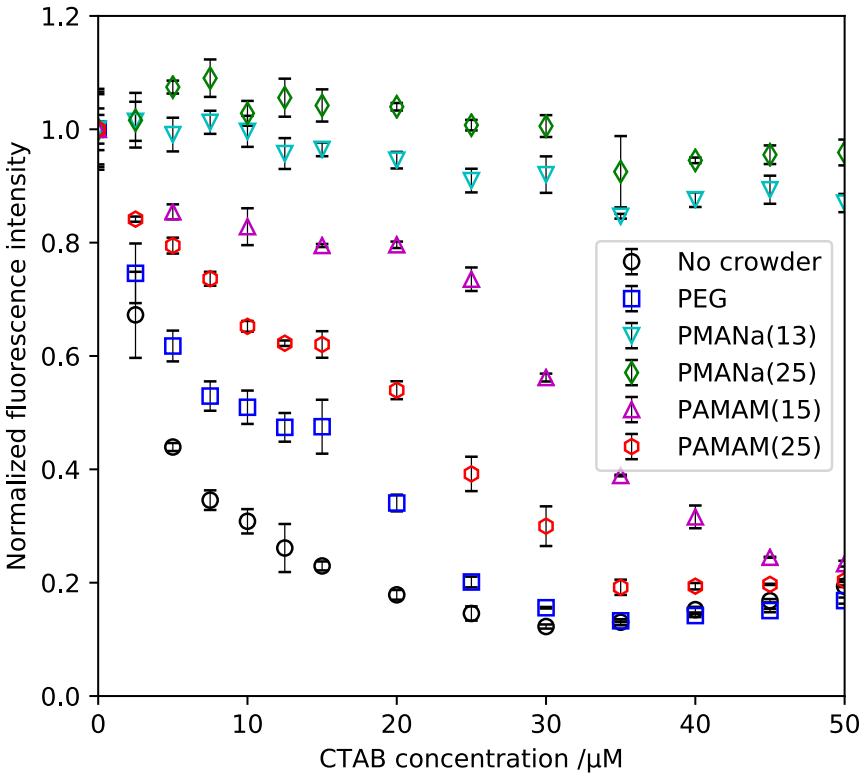

Figure 5.1: Normalised fluorescence intensity from DNA-GelStar complex in the absence of crowder (black circles) and in the presence of either 25 mg/mL PEG (blue squares), 13 mg/mL PMANa (cyan tringles), 25 mg/mL PMANa (green diamonds), 15 mg/mL PAMAM-OH (purple triangles) or 25 mg/mL PAMAM-OH (red hexagons), as a function of increasing concentration of CTAB. The data is the same as presented in Fig. 4.11, but the fluorescence is normalised the resepective sample series with 0 µM CTAB. The results are based on triplicates and presented as mean with error bars, indicating the standard deviation. Results shown by the black circles and purple triangles were obtained during the project assignment in the fall of 2019.

5.2.1 A neutral linear polymer: PEG

Experimental approach

PEG was first described to induce DNA condensation in 1971 [35]. Using PEG with the same length but a much longer DNA (T4 16.7 kbp), condensation was found using 250 mg/mL and 10 mM buffer [63]. Apart from the size of the DNA, the dimensions and characteristics of the crowding molecules are of importance [64, 65]. It is thus not surprising

that the addition of PEG up to a concentration of 180 mg/mL does not fully condense DNA (Fig. 4.10a). It was however surprising that fluorescence intensity increases when the concentration of PEG increases (up to $I/I_0 = 1.6$). Fluorescence measurements presented in Table 4.1 do confirm that the fluorescence from GelStar in solution is affected by the presence of PEG ($I/I_0 = 0.051$), however, the increase is not entirely justified by it (up to 0.15 for the used PEG concentration). PEG solutions are known to have a dielectric constant lower than that of water [66]. Increasing the PEG concentration would lead to a strengthening of the electrostatic interaction (Eq. 2.3), which suggests that the GelStar may interact via Coulomb interaction with the DNA, and the increase in fluorescence is a consequence of this. Since the intensity increases with addition of PEG, one can assume that the observed decrease in intensity at 140 mg/mL is due to DNA condensation induced by PEG.

For practical reason it was chosen to work with 25 mg/mL of PEG. As discussed, this concentration does not lead to DNA condensation as observed with dye exclusion assays (Fig. 4.10a), EMSA (top panel of Fig. 4.13) and it did not protect DNA against enzyme digestion (top panel in Fig. 4.15). The addition of PEG to the pre-equilibrated DNA-CTAB complexes did not result in an increased DNA condensation when studied using dye exclusion assays. In fact, the presence of PEG lead to a smaller condensation degree (less condensation) at intermediate CTAB concentrations (blue and bøack symbols in Fig. 5.1), which was surprising. However the CTAB concentration at which DNA is fully condensed is not very different in the absence and presence of PEG. This indicates that 25 mg/mL PEG is not a high enough concentration to induce DNA condensation by crowding, but one expects an enhanced effect if the PEG concentration is increased.

The results from EMSA do show increased DNA condensation by CTAB in the presence of PEG under the conditions of the experiment (Fig. 4.13). With PEG the DNA band becomes broader at a lower concentration of CTAB compared to its absence. This effect is more prominent at higher concentrations of CTAB, where a larger fraction of the DNA is unable to migrate from the well due to condensation. The contradictory results obtained using dye exclusion assays and EMSA could be an effect of the increased concentration of DNA employed in EMSA, which yields a more crowded system, possibly enhancing the effect of PEG.

Macromolecular crowding induced by PEG has been shown to enhance the reaction rate of DNase I [67]. Results from DNase protection assay using PEG as a crowding molecule, shown in the top panel in Fig. 4.15, clearly show that DNA is less protected from DNase I in the presence of PEG. This could be due to both the concentration of PEG not being high enough to condense DNA, and the presence of PEG enhancing the interaction between DNA and DNase I. This effect is particularly evident up to 100 μM CTAB, but as the concentration of CTAB increases the small DNA fragments are no longer visible in the gels. This could be due to the protection of DNA by the CTAB and/or to the condensation of the DNA fragments by the CTAB. To distinguish between these phenomena, one would need to extract the CTAB from the DNA after digestion and before running the gel.

Modeling approach

The addition of PEG to DNA shifted the size distribution of the latter to slightly larger R_G (Fig. 4.1) indicating that the DNA has a slightly more expanded shape. The neutral crowders in this model are only space filling, i.e. inert crowders, and since their volume fraction is so small, namely 0.0015 taking into account the monomer hard-sphere radius, the model DNA is still able to maintain its regular conformation. This slight shift in the size distribution has been shown in previous work [68], and seeing as it has been reported that a volume fraction up to 0.2 does not condense DNA [69], this is consistent with previous results.

The presence of inert polymers could enhance self-assembly of CTAB. With a non-ionic polymer the CAC has been found to be lower than the CMC, but with comparable values [70]. Therefore, the amount of CTAB would need to be very close to the CMC for the addition of PEG to induce CTAB self-assembly. Since PEG is neutral there is no interaction with CTAB and, as can be seen by the rdf of CTAB – CTAB pairs in Fig. 4.5a, no self-assembly occurs in System CP_0 (see also snapshot in Fig. 4.6b).

The addition of both PEG and CTAB causes DNA to have a more compact form, compared to System DP_0, however, the size distribution of DNA is shifted towards larger values compared to System DC (Fig. 4.1). Spherical neutral crowders and model H-NS, with an interaction potential of 1kT, have been shown to highly condense the DNA [68],

however no significant effect was observed when changing the volume fraction of the crowders from 0 to 0.16. Considering that the volume fraction of PEG used in this work is lower, one would expect a similar result, in which the size distribution of the DNA was not affected. Instead, the result obtained here suggests that PEG opposes DNA condensation by CTAB.

Investigating the snapshot of System DCP_0 (Fig. 4.2f), it can be seen that the DNA is very tightly wrapped around the micelles, forming an elongated complex. The contact analysis between DNA monomers and CTAB headgroup also indicate that a large fraction of the monomers are in contact with two micelles, however the central monomers are not in contact with more, which was the case in the absence of PEG. This elongated complex is the reason for the larger radius of gyration of the model DNA in System DCP_0 compared to DC. Since the crowders are evenly distributed in the system, their presence could constrain the conformation in which the DNA wraps around the micelles. Without the crowders, the DNA can interact with the micelles freely and can bend inwards to the center of the system. It would be interesting to follow the experimental procedure more closely and add the PEG after DNA-CTAB equilibration. It should also be noted that the differences in the DNA-CTAB complexes may represent minima in the energy landscape. These systems are very large and the interactions between some of the elements very strong, which leads to a large number of rejections by hard-sphere overlap. The acceptance of DNA monomers is about 7% and that of CTAB tail end monomer is 11%, which attests the equilibration problem. Future work should include the implementation of more efficient MC moves and/or annealing procedures for improved equilibrations. The addition of the different crowder agents to a pre-equilibrated DNA-CTAB complex would have helped in the interpretation of the results.

5.2.2 A linear polyanion: PMANa

Using as a motivation the fact that most macromolecules in the cell are negatively charged, the effect of a linear polyanion on the DNA-CTAB interaction was looked upon.

Experimental approach

Starting with systems containing only DNA and polyanions, negatively charged macromolecules are also expected to induce DNA condensation above a certain concentration due to the excluded volume effects plus the electrostatic repulsion between the crowders and DNA. Results from dye exclusion assays show that DNA starts condensing at 100 mg/mL PMANa, which is lower compared to PEG that required 120 mg/mL for the intensity to start decreasing (Fig. 4.10a). Since the molecular weights of PEG and PMANa are very similar, this slight condensation must be an effect of the electrostatic repulsion between DNA and PMANa. This is in good agreement with the results from the modeling (see below).

Again, it was decided to work with 25 mg/mL PMANa, which by itself does not visibly affect the DNA conformation using dye exclusion assays, EMSA and DNase protection assays. However, the addition of PMANa to DNA+CTAB samples lead to interesting results. Considering CTAB and PMANa only, the electrostatic interactions between CTAB and PMANa should lower the CTAB concentration at which the CTAB starts aggregating. Indeed, it has been shown that the CAC of CTAB in the presence of 1 mg/mL PMA at pH 8 is 50 μM, evaluated using the photophysics of pyrene [71], which is lower than the CMC of CTAB (0.9 mM). Studies have also showed that the CAC of C_{10}TAB increases with increasing concentration of PMA, and therefore one would expect the CAC in this case to be somewhat higher since a concentration of 25 mg/mL PMANa is employed instead. Electrostatic repulsion between DNA and PMANa, will aid in the condensation of DNA, but since PMANa interacts with CTAB, this could oppose condensation. Indeed, results from dye exclusion assays (Fig. 5.1) show that PMANa fully inhibits DNA condensation by CTAB up to a CTAB concentration of 300 μM (only results up to 50 μM are shown), which suggests that PMANa interacts strongly with CTAB, and inhibits its interaction with DNA. One would expect DNA to start condensing when CTAB would be in excess compared to PMANa, however that point is never reached in these experiments. Dye exclusion assays were also performed using 13 mg/mL PMANa, which yields a charge concentration of 120 mM (similar to the charge concentration of PAMAM-OH at 25 mg/mL). However, the excess of charge was still large and no decrease in fluorescence was observed.

Unfortunately, the results from EMSA were inconclusive. The results from the reference samples are very different compared to the results from reference samples in all other EMSA studies (see lanes 2-8 in middle panel compared to top and bottom panels). Lane 13 also presents a much higher intensity than the other. Comparing lanes 10-16 in the top and middle gels, it can be seen that the PMANa opposes DNA condensation up to roughly 300 μM but the samples at 500 μM and 800 μM CTAB seems to be fully condensed. Due to the large charge excess present one would expect that a larger concentration of CTAB would be needed to fully condense DNA. Anyhow, this experiment should be repeated in order to strengthen the discussion.

The results from the DNase protection assay with PMANa were equally disappointing. While the control samples in the absence of crowders look consistent (lanes 1-8 in all gels in Fig. 4.15), the results for the DNA digestion look very different. One feature in particular is the fact that the DNA band is skewed to the left (also visible in the assay at 100 μM, Fig. 4.16, and to a much lesser extent in the EMSA, Figs. 4.13 and 4.14), and that all bands in the gel, if present, show the same lower end, which is also the case in all gel electrophoresis performed in samples containing PMANa. This suggests that the PMANa interfers with the diffusion of the DNA in the bands, which makes it difficult to discuss the results. The apparent lack of smaller DNA molecules, which indicate digestion, could be due to the mentioned interference of PMANa in the band migration, or to the inhibition of the DNase I enzyme by the PMANa due to perhaps a direct interaction between them. The near disappearance of the bands at CTAB concentrations of 500 and 800 μM is consistent with the same phenomenon observed for EMSA in Fig. 4.13.

Modeling approach

Negatively charged linear polymers, such as PMANa, will have a more elongated shape and be more distributed in the cell, compared to PEG, due the electrostatic repulsions between the monomers of the chain and between the crowders, respectively. This is shown by the larger R_G of PMANa (Fig. 4.9b) and the shifting of the rdf of PMANa – PMANa pairs to larger values (Fig. 4.8b).

The addition of negatively charged crowders to DNA will lead to electrostatic repulsion between the crowders and DNA. The rdf of DNA – PMANa pairs show that the

crowders are in average more distant from the DNA, compared to PEG. The electrostatic repulsion causes the crowders to have a slightly more compacted form (Fig. 4.9b) and the maximum in the rdf of PMANa – PMANa (center of mass) shifts to lower values (Fig. 4.8b), however not to the extent of the values observed for PEG. Due to this, in addition to the effect from electrostatic repulsion, one would expect a larger crowding effect from PMANa than from PEG. The R_G distribution of DNA is indeed found to be smaller in the presence of PMANa (Fig. 4.1), which is likely due to the negative charge of the crowders, and not the excluded volume itselt, due to the small volume fraction of the crowders in these systems, as discussed.

CTAB has a positively charged headgroup and therefore the addition of negatively charged crowders will lead to electrostatic interactions between the crowders and CTAB. The CAC of a CTAB-polyanion system is much lower than that of a CTAB-(neutral) polymer one, due to the electrostatic interactions. The rdf of CTAB – PMANa pairs (Fig. 4.8g) show that the interaction between these components is much stronger than the interaction between CTAB and PEG. Similarly to adding DNA to CTAB, the CTAB self-assembles into micelles in the vincinity of PMANa, which is shown by the rdf of CTAB – CTAB pairs (Fig. 4.5a) and the formation of large clusters (Fig. 4.7a). However, the self-assembly is more prominent in System DC, which is seen by comparing the height of $g(r)$ of CTAB – CTAB pairs, and by noting that the CTAB self-assembles into micelles with lower aggregation numbers (compare the green curves in Figs. 4.7a and 4.7b). Since there is a strong interaction between CTAB and PMANa, where multiple crowders wrap around the clusters (see snapshot in Fig. 4.6c), CTAB affects the conformation of and the average separation between the crowders. The rdf of PMANa – PMANa pairs show a very large peak at very low crowder (center of mass) separations (Fig. 4.8b), and the size distribution indicates two populations of crowders, one that is more condensed by the association with CTAB and one that resembles that of freely moving PMANa molecules (Fig. 4.9b). Note that this occurs even if the CTAB molecules are in excess, charge-wise (960 CTAB headgroups versus 640 PMANa monomers).

Both DNA and PMANa are shown to strongly interact with CTAB, inducing its self-assembly in Systems DC and CP_L, and so the polyanion could oppose the condensation of DNA by CTAB. It is found that, in System DCP_L, the PMANa does not interact as

strongly with CTAB which is seen by the change in rdf of CTAB – PMANa pairs in Fig. 4.8h. However, there is still some interaction, which lowers the interaction between DNA and CTAB (Fig. 4.3). The contact analyses show that in average the number of CTAB headgroups along the DNA molecule decreases when compared with Systems DC and DCP_0 (Fig. 4.4). The size distribution of DNA is shifted towards larger values compared to the system in the absence of crowder, which could be due to the competition with PMANa towards the CTAB, but could also be due to the differences in the equilibration of the DNA-CTAB complex, as discussed above. The conformation of the crowders is affected, causing them to have a slightly lower R_G compared to the free PMANa (System P_L), however they are not as compacted as in System CP_L. The average separation between the crowders resembles the rdf of PMANa – PMANa in both Systems P_L and DP_L (Fig. 4.8b).

While it is clear that some interaction between the PMANa and CTAB is present in the presence of DNA, this is not enough to exclude the CTAB from the DNA as it was observed in the experimental part. This could be due to the fact that a lot fewer crowders are present in the simulations (0.67 in the modelling versus a 150 fold excess in the experimental part, taking the lower investigated charge ratio of both PMANa monomer and CTAB headgroups) and/or that the chosen description of the DNA and CTAB models overestimate the interaction between these components. The discrepancy can also be due to the fact that PMANa is modeled using a similar angular force constant as DNA, but in reality the PMANa has a lower persistence length compared to DNA, and a more flexible chain can interact more efficiently with the CTAB aggregates.

5.2.3 A branched polyanion: PAMAM-OH

Seeing as a large amount of the macromolecules and macromolecular complexes in the bacteria cell are negatively charged and has a spherical-like conformation (e.g. ribosomes), the effect of negatively charged dendrimers on the DNA-CTAB interaction was investigated. Dendrimers were chosen due to their compact, spherical conformation and size monodispersity.

Experimental approach

When adding PAMAM-OH to DNA one would expect the latter to condense above a certain concentration due to excluded volume effects and electrostatic repulsions, as was observed with PMANa. Results from dye exclusion assays do show that at a concentration of 100 mg/mL PAMAM-OH, the highest studied, the DNA had not yet started to condense, while a slight condensation was observed with PMANa for the same concentration. However, since the charge concentration of PAMAM-OH at 100 mg/mL is 495 mM, which is much lower than the concentration of 926 mM at 100 mg/mL PMANa, it is not surprising that DNA condensation is not achieved. In addition, due to the distribution of their monomers, the dendrimers are smaller molecules, which reduces their crowding effects.

Adding dendrimers when using CTAB as a condensing agent, could increase DNA condensation due to, again, excluded volume effects and electrostatic repulsion. However, since the dendrimers are negatively charged one would also expect it to compete with the DNA in the interaction with CTAB, as was observed with PMANa. Results from dye exclusion assays with 15 mg/mL PAMAM-OH (purple triangles in Fig. 5.1)(obtained during the project in the fall of 2019) show that the presence of dendrimers somewhat opposes DNA condensation by CTAB, compared to in the absence of crowders. Increasing PAMAM concentration seems to decrease the opposing effect on DNA condensation (Fig. 5.1). Considering that the dendrimers are in large excess compared to the charge of CTAB, this indicates that even if the interaction between PAMAM-OH and CTAB may increase, the excluded volume and electrostatic repulsion between DNA and PAMAM-OH seem to be more dominant. This suggests that further increase in the concentration of dendrimers could at some point enhance DNA condensation.

The charge concentration at 25 mg/mL PAMAM-OH and 13 mg/mL PMANa is 124 mM and 120 mM, respectively. As discussed with PMANa, dye exclusion assays clearly showed lack of DNA condensation (up to 300 μM), which is likely due to the large excess of PMANa compared CTAB. Therefore it is very interesting to find that the same charge concentration of dendrimers does not offset DNA condensation to the same extent as PMANa.

EMSA studies were done to investigate the effect of adding PAMAM-OH dendrimers

to DNA-CTAB complexes. Unfortunately the intensity of the bands is very low in this gel (lower panel in Fig. 4.13) and these are difficult to compare. Anyhow, the onset of condensation seems to occur at similar concentration in the absence and presence of PAMAM-OH, but complete condensation is only achieved at larger CTAB concentrations when PAMAM-OH is present. The observed delay in the offset of DNA condensation induced by CTAB due to the presence of PAMAM-OH in the dye exclusion assays was not observed in EMSA. This could be due to the difference in experimental conditions (e.g. higher DNA concentration and ionic strength) and/or the large interval between the samples. The apparent amplification of DNA condensation at larger CTAB concentrations was not seen in the previous assay, but such CTAB concentrations were not tested.

Seeing as no DNA condensation was observed by adding 25 mg/mL PAMAM-OH in dye exclusion assays (Fig. 4.10a), one would not expect protection of the DNA by adding this concentration of crowder. However, the gel in Fig. 4.15 (bottom panel) shows that DNA is less digested in the presence of PAMAM-OH. This may be due to a direct interaction of the DNase with the PAMAM-OH. On the other hand, when increasing the concentration of CTAB there is an opposite effect where the dendrimers slightly enhance DNA digestion, as seen by the lower intensity from the bands, even if they have migrated a similar distance than the samples in the absence of crowder. Such lack of protection is caused by the lower condensation of DNA, which is consistent with results obtained in dye exclusion assays and EMSA.

Modeling approach

A branched polymer with negative surface charges was used to model a PAMAM-OH generation 2.5 dendrimer to assess the effect of negatively charged spherical-like macromolecules in DNA condensation within a bacteria cell. The rdf of $\mathrm{PAMAM}_{\mathrm{mon}_1} - \mathrm{PAMAM}_{\mathrm{mon}_5}$ (central and surface monomer) pairs shows that their average separation is 25 Å, indicating that radius of the model PAMAM molecule is approximately 25 Å. The radius of PAMAM is lower compared to the R_G of PMANa ($\sim$ 60 Å), and since they possess the same number of charged monomers, PAMAM has a larger charge density.

The volume fraction of PAMAM crowders is, based on the radius, found to be only 0.0115, which is quite low compared to the reported volume fraction of 0.2 that is needed

to condense DNA. However, seeing as some condensation was observed by adding PMANa one would expect a similar shift in the size distribution of the DNA when adding PAMAM. Indeed, the results show that the presence of PAMAM enhances condensation of DNA, compared to both the absence of crowders and the presence of PMANa, where the former is caused by the electrostatic repulsion between DNA and crowders, and the latter may be due to the increased charge density of the PAMAM crowders compared to the PMANa.

Addition of PAMAM crowders to CTAB should lead to interactions between the surface monomers of PAMAM and CTAB headgroups, which is evident from the rdf of CTAB – PAMAM pairs (Fig. 4.8i). As discussed above, the interaction between a negatively charged polymer and CTAB will cause self-assembly of the CTAB molecules, and indeed the rdf of CTAB – CTAB pairs show that CTAB-molecules self-assemble in the presence of PAMAM. The PAMAM-induced CTAB self-assembly is similar to that observed with PMANa, with the formation of micelles with approximately similar aggregation numbers (with the exception of some smaller aggregates), which is likely due to the fact that they have the same number of charged monomers. There are, however, some differences, as can be appreciated in the snapshots of Systems CP_S and CP_L (Figs. 4.6c and 4.6d). Whereas the PMANa crowders wrap around the micelles, the PAMAM crowders induce the formation of micelles on their surface, which in turn attract other dendrimers (Fig. 4.8c). Such CTAB-induced crowder aggregation is also observed in the PMANa system (Fig. 4.8b). It is clear that the conformation of the branched crowders is not affected by the interaction with CTAB. The larger conformational entropy of the linear chain allows for a better matching of the charges and stronger interaction with the CTAB. In fact, the two-body potential between the CTAB headgroups and charged monomers of PMANa and PAMAM was found to be -10 and -8.9 kJ/mol, respectively, which also may explain why PMANa is able to extract CTAB from DNA as observed in dye exclusion assays.

PAMAM crowders could enhance DNA condensation by CTAB, as was observed in the absence of CTAB. However since PAMAM has been shown to interact strongly with CTAB this could oppose DNA condensation, as seen in the dye exclusion assays. As was observed with PMANa, the interaction between PAMAM and CTAB decreases upon the addition of DNA. However, there is still some interaction as shown in the $g(r)$ of the CTAB

– PAMAM pairs (Fig. 4.8i), and the decrease in $g(r)$ of DNA – CTAB pairs (Fig. 4.3). In System DCP_S, Fig. 4.5b indicates that less CTAB molecules are present in aggregates, and the aggregation number of the micelles also changes, where fewer and larger micelles are formed in the presence of both DNA and PAMAM . The contact analysis indicates that fewer DNA monomers are in contact with several micelles and a few monomers are in fact in contact with no CTAB molecules. Investigations of multiple snapshots (Fig. 4.2h) show that since the micelles have a larger aggregation number, the DNA wraps multiple times around one single micelle, which explains the noticable difference in contact analysis.

Since PAMAM interacts with CTAB, causing a decreased interaction between DNA and CTAB, one would expect this to oppose DNA condensation. However, the distribution of the R_G of DNA when adding PAMAM decreases compared to both the absence of crowder and presence of PEG or PMANa. The enhanced DNA condensation effect observed for the spherical crowders compared to the linear ones may be an affect of the higher charge density of PAMAM crowders, which also yielded a slightly larger condensation of DNA in the absence of CTAB, as well as the inability of the PAMAM to extract the CTAB from the DNA. However, as discussed above, the size distribution of the DNA in the presence of both CTAB and crowders seems to be highly affected by the fact that DNA is unable to efficiently bend as it interacts with and wraps around the micelles, which rises the question on whether or not the true potential energy minimum was reached in these systems. Future work should therefore, as suggested above, add crowders to an equilibrated DNA-CTAB complex to fully be able to compare the effects of various crowder molecules.

To summarize, the experimental data suggests that PAMAM-OH oppose DNA condensation by CTAB at low CTAB concentration, but at higher concentrations it is as good or better than PEG, at the same concentration. At large CTAB concentration, where DNA is close to fully condensed, PAMAM enhances this state due to excluded volume effects, highlighted by their charged surface. The simulations show, that for the chosen models, PAMAM competes weakly with the DNA for the CTAB. The modeling appears to be in excellent agreement with the experimental results, but the same model was not able to predict the experimental results obtained for PMANa, as discussed in

previous section.

5.3 DNA condensation by CTAB at high ionic strength

Increasing the concentration of salt leads to the screening of electrostatic interactions in a solution. Salt screens the electrostatic interactions between the DNA segments, which decreases the persistence length of the DNA, aiding in the condensation process. On the other hand, increasing salt concentration will lead to a weakening of the interaction between a cationic condensing agent and DNA, which has been shown to increase the concentration of spermidine needed to induce DNA condensation [72]. Therefore, the effect of salt is expected to increase the required concentration of CTAB to condense DNA.

In this work, 100 mM NaBr was employed to increase the ionic strength of the system. The results from dye exclusion assays (Fig. 5.2) show that DNA condenses at a higher CTAB concentration upon the increase of ionic strength. This indicates that salt has a greater effect on opposing DNA condensation by cationic condensing agent, compared to the enhanced effect from decreasing the persistence length.

The delay in DNA condensation by CTAB upon increased salt concentration should also be evident in EMSA results, however the DNA seems to be condensing at 100 μM CTAB (Fig. 4.14), which is similar to the results at low ionic strength. This does not mean that the salt did not affect the required CTAB concentration to induce DNA condensation, but it may happen the variation in this concentration is within the range 50 to 100 μM. Experiments probing this interval should be conducted in the future. It should be mentioned that the gel electrophoresis setup involve the placement and running of the samples in a gel within a tank filled with a buffer with an ionic strength of 20 mM. It is thus possible that the samples equilibrate in the new environment, which would explain the lack of differences between the samples at low and high ionic strength.

DNase activity is very dependent on the presence of Mg^{2+} and Ca^{2+}, however this was not employed to avoid effects from these ions on DNA condensation. Na^{+} has been shown to lower the activity of DNase I. Therefore, increasing the ionic strength in DNase protection assay should lead to less digested DNA. Indeed, the results from DNase protection assay clearly show that DNA digestion is somewhat hindered at high ionic strength (compare lanes 1 and 2 in Fig. 4.15 with those of Fig. 4.16). Although the results are

not shown in the same gel, and one should compare gels with caution, there is a clear distinction between the results at low ionic strength where almost all DNA are digested, compared to at high ionic strength, where the DNA is nearly not digested at all. This can be seen by the intensity of the band resembling that of undigested DNA and of the band overlapping that of DNA alone, indicating a large number of molecules with the same size as the undigested sample. This effect is therefore suggested to be due to the decreased activity of DNase I in the presence of Na^+.

5.4 Effect of salt addition in DNA-CTAB-crowder systems

Considering that DNA condensation by neutral polymers is expected to be facilitated by the presence of salt, and that electrostatic interactions are very important in the systems with negative crowders, experimental work was conducted to assess the effect of a higher ionic strength in these systems.

Even though the increase in fluorescence induced by the presence of DNA and crowder molecules in dye exclusion assays was not that significant at high ionic strength, it is assumed that a decrease in fluorescence indicates DNA condensation, and it is the trends of the result that will be discussed. Therefore, a renormalisation of the results obtained in dye exclusion assays are shown in Fig. 5.2.

5.4.1 A neutral linear polymer: PEG

Using PEG with the same length as the one used in this work, but a much longer DNA (T4 16.7 kbp), DNA condensation was observed using 45 mg/mL and 1 M of salt, whereas in 10 mM buffer 250 mg/mL PEG was needed to induce condensation [63]. The presence of large concentrations of salt improve DNA condensation since the electrostatic repulsions within and between the DNA chains are screened. This was later termed polymer salt induced (psi-Ψ) condensation [39]. Results from dye exclusion assays show that DNA starts condensing at 140 mg/mL PEG both in the absence and presence of 100 mM NaBr (see Fig. 4.10a and 4.10b). However, above this concentration the drop in fluorescence intensity with PEG concentration is larger in the presence of salt, which shows the coop-

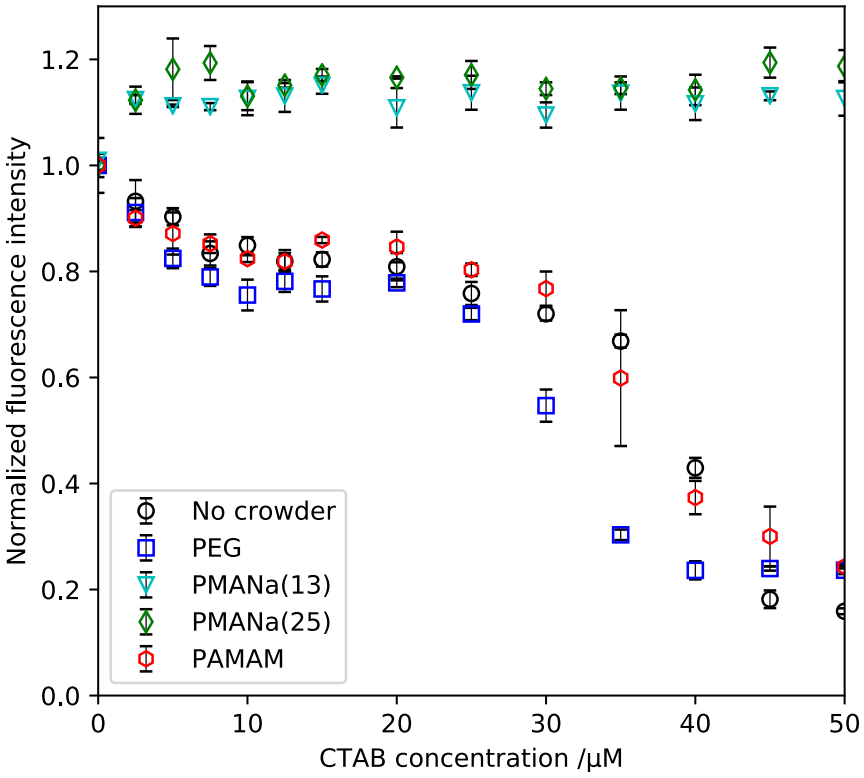

Figure 5.2: Normalised fluorescence intensity from DNA-GelStar complex (in 100 mM NaBr) in the absence of crowder (black) and in the presence of either 25 mg/mL PEG (blue squares), 13 mg/mL PMANa (cyan diamonds), 25 mg/mL PMANa (green diamonds) or 25 mg/mL PAMAM-OH (red hexagons), as a function of increasing concentration of CTAB. The figure shows the same data as Fig. 4.12, however the fluorescence is normalised to samples at 0 μM CTAB. The results are based on triplicates and presented as mean with error bars, indicating the standard deviation.

erative Ψ-condensation when increasing the ionic strength. The normalised fluorescence is not purely dependent on the exclusion of the dye, i.e. DNA condensation, but seeing as the intensity has a lower value at 180 mg/mL it is here assumed that this indicates a more condensed state of the DNA.

When using CTAB as a condensing agent, salt will, as discussed above, lower the interaction between CTAB and DNA, which will oppose DNA condensation. On the other hand, Ψ-condensation is expected to enhance condensation as shown above. Results from dye exclusion assays (Fig. 5.2) show that the screening of electrostatic interactions between DNA and CTAB predominate in this systems. The presence of both PEG and NaBr induces DNA condensation at a slightly lower concentration of CTAB, however the effect of Ψ-condensation is not very noticable, which is likely due to the low concentration

of both PEG and NaBr employed here.

Looking at the results from EMSA on the other hand, one sees that PEG seems to oppose DNA condensation at lower concentrations of CTAB, however, a higher degree of DNA condensation is reached at a lower concentration of CTAB in the presence of PEG. The effect of Ψ-condensation is thus not very noticable, as was observed in dye exclusion assays. As discussed above, the ionic strength of the running buffer in these experiments may affect the results and minimize the variations between the systems with different ionic strength.

DNase activity decreases when the ionic strength increases by addition of Na^+, whereas the addition of PEG will enhance activity if the DNA is not protected, as discussed above. DNase protection results show that addition of PEG enhances cleavage of DNA, which is reasonable since results from dye exclusion assays showed that 25 mg/mL PEG at high ionic strength is not enough to condense DNA. Furthermore, as discussed above, mild crowding conditions are known to induce the activity of enzymes. Consistently with the results at low ionic strength, it is seen that the presence of PEG leads to a weaker protection at low CTAB concentrations, however at higher CTAB concentrations the low intensity of the DNA bands could indicate less protection by CTAB and/or a decreased intensity due to the higher amount of DNA-CTAB complexes contained in the well (which was also observed in EMSA).

To summarize, it was found that 100 mM NaBr lead to an increase in CTAB concentration needed to condense DNA. Under the used conditions, the addition of PEG to DNA+CTAB samples with 100 mM NaBr did not lead to a clear trend in the results. Dye exclusion assays show a more efficient DNA condensation at intermediate CTAB solution, and EMSA show a shorter CTAB concentration range between samples that show a change in DNA band mobility (DNA condensation start) and the absence of bands (full DNA condensation), compared to in the absence of crowder.

5.4.2 A linear polyanion: PMANa

Increase in ionic strength will yield a lower effect on DNA condensation from negatively charged crowders, which has been shown with the negatively charged protein BSA, where unfolding of the DNA was observed when the concentration of salt was increased [40]. This

is an effect of the screening of the electrostatic repulsions between DNA and negatively charged crowder. This is hinted at when considering that 100 mg/mL PMANa leads to some decrease in fluorescence in the dye exclusion assays at low salt concentration (Fig. 4.10a), but no condensation was observed at this concentration at high ionic strength (Fig. 4.10b).

Addition of PMANa to DNA-CTAB solutions at low ionic strength did show that PMANa interacts very strongly with CTAB, hence no DNA condensation was observed in dye exclusion assays up to 300 μM. Increasing the ionic strength of these solution will yield three effects due to screening of the electrostatic interactions: (i) it will lower the interaction between PMANa and CTAB, which could enhance DNA condensation due to the increased amount of free CTAB that can interact with DNA; (ii) it will decrease the interaction between DNA and CTAB, as observed in the absence of crowder; and (iii) it will decrease the effect of the excluded volume of the crowder, which is likely very negligable since only a slight difference was observed when increasing the ionic strength in the absence of the cationic condensing agent. Results from dye exclusion assays show that, again, no DNA condensation is observed up to 300 μM CTAB in the presence of both 13 and 25 mg/mL PMANa (Fig. 5.2), which indicates that PMANa still interacts strongly with CTAB.

On the other hand, whereas PMANa fully inhibited DNA condensation up to 300 μM in dye exclusion, results from EMSA show that DNA condensation is not fully inhibited and, in fact, DNA starts condensing at 300 μM, with a CTAB to DNA charge ratio $r_{charge} = 2.6$ which is significantly lower than as was observed with dye exclusion assay. As discussed in Section 5.2.2. for the low ionic strength case, the PMANa seems to interfere in this experimental setting, which may explain the differences observed between the techniques.

The apparent interference of PMANa on DNA mobility or directly on the activity of the DNase I, makes it also difficult to interpret the results from the protection assay. Anyhow, it can be seen that increasing the salt concentration significantly increased the protection of DNA in reference samples (lanes 1 and 2 in middle gel in Fig 4.16). In the presence of PMANa the shape of the band is not changed but the intensity is much lower, indicating some level of digestion of the DNA. The lower activity of DNAse I is evident

in the samples at lower CTAB concentration. It can be noticed that the fluorescence intensity in the wells is low compared to the systems without PMANa, also indicating that there was a lower DNA protection, which is as expected seeing as EMSA results only indicated slight formation of larger and/or neutral DNA-CTAB complexes in the presence of PMANa.

Increasing the ionic strength of the systems by 100 mM did not lead to significant changes when compared with the neutral polymer in the same conditions. PMANa is still found to hinder, or at least weaken the interaction between DNA and CTAB, affecting DNA condensation.

5.4.3 A branched polyanion: PAMAM-OH

It was shown that the screening of the electrostatic interaction between PMANa and DNA will require a higher concentration of crowders being needed to induce DNA condensation. Results from dye exclusion assays of the DNA-PAMAM-OH systems at high ionic strength were not obtained, but seeing as 100 mg/mL PAMAM-OH, at low ionic strength did not cause condensation, one expects a similar effect as that observed with PMANa, where a higher concentration of negatively charged crowder is required to induce DNA condensation.

When adding CTAB, the increase in the ionic strength was expected to lead to a similar effect as observed without crowder, that is, a larger concentration of CTAB being required to induce the same levels of DNA condensation. Following the used assumption that a decrease in I/I_0 corresponds to DNA condensation is was found that at low ionic strength a CTAB to DNA charge ratio of 5.7 was required to fully condense DNA (with PAMAM-OH), while at high salt concentration full DNA condensation was observed at a charge ratio of 8.1. This shows that the presence of salt increases the required amount of CTAB to induce DNA condensation expected. It is also shown that at higher ionic strength, adding PAMAM-OH only does slightly delay DNA condensation by CTAB compared to in the absence of crowder (black vs red symbols in Fig. 5.2). Since the impact of adding dendrimers was much higher at low ionic strength, it suggests that the weaker delay in DNA condensation, observed at high ionic strength, is an effect of the decreased interaction between crowder and CTAB. It would therefore be interesting to investigate if

further increase in salt concentration would lead to enhanced DNA condensation by the presence of dendrimers.

EMSA was conducted to further investigate the effect of dendrimers on DNA condensation. The results show that the dendrimers slightly prevent formation of larger and/or neutral DNA-CTAB complexes at low concentrations of CTAB, but as the CTAB concentration increases the DNA seems to be more condensed in the presence of PAMAM-OH (bottom gel in Fig. 4.14). As discussed above, the running buffer may affect the ionic strength of the solution, and may explain why one observes more DNA condensation with PAMAM-OH in EMSA, compared to in dye exclusion assays, where no significant effect on DNA condensation was observed when adding dendrimers.

25 mg/mL dendrimers were shown to aid in the protection of DNA towards enzyme digestion at low ionic strength. However, at higher ionic strength, the level of protection of DNA-CTAB complexes seems slightly lower in the presence of PAMAM-OH, which is consistent with results from EMSA and dye exclusion assays where less DNA condensation was observed at intermediate CTAB concentrations. At higher CTAB concentrations no significant effect is observed on the protection of DNA. However, seeing as more neutral and/or larger complexes are formed in the presence of dendrimers, which yielded less migration from the wells at higher CTAB concentrations in EMSA, the DNA may be slightly more protected at high concentrations of CTAB since the bands have a similar intensity and EMSA show that more of the sample may be contained in the well. Either way, the presence of dendrimers does not indicate a large effect on the protection of DNA, which is consistent with both results from dye exclusion assays and EMSA.

To summarize, PAMAM-OH dendrimers were found to slightly affect the DNA condensation by CTAB. The dendrimers compete with DNA for the CTAB and so larger concentration of CTAB are required to induce the same condensation level as in the absence of crowder. The addition of salt seems to decrease this opposing effect, such that the differences between the dendrimers and the linear (neutral) polymer are not that large, and very different from the linear polyanion, which is able to hinder DNA condensation much more efficiently.

Chapter 6

Conclusion

6.1 Summary

In this work, crowder molecules with different characteristics were studied to evaluate their effect on the condensation of DNA by cationic amphiphilic molecules. The concentration of crowders was not large enough to qualify for the crowded conditions observed in cells, but some interesting trends were nevertheless observed. It was found that, under the studied conditions, PEG, a linear neutral polymer weakly enhances DNA condensation by CTAB, particularly at high salt concentrations. Using negatively charged crowders enhances the condensation of DNA, due to the electrostatic repulsion, but in the presence of CTAB, the crowder competes with the DNA for the binding to the surfactant and DNA condensation is hindered. This opposing effect was found to be more evident for the linear than the spherical-like crowder. The delay in DNA condensation by CTAB due to dendritic polyanion is somewhat decreased in the presence of salt, but the linear one does seem not to be affected by the used salt concentration, which highlighted the differences between the two. It is suggested that the flexible and adaptable linear polyanion is able to interact with CTAB more strongly than the dendritic polyanion, as confirmed by the simulation results, making it able to compete more efficiently with the DNA for the CTAB binding.

Monte Carlo simulations also showed that negatively charged crowders enhance DNA condensation, whereas no effect was observed with neutral crowders due to the low volume fraction of the crowders, which is in good agreement with the experimental work. With a model CTAB as condensing agent, the presence of neutral or negatively charged

linear crowder molecules was found to oppose DNA condensation, whereas an enhanced effect was observed with the spherical-like crowder molecules. Unfortunately, the studied systems were not very dynamic, which, together with the large number of particles and limited time, means that they may not have reached equilibrium. This would explain the discrepancy between the modelling and experimental results.

CTAB is used in this work as a model for NAPs, due to the comparable DNA condensation mechanism, that is, self-assembly at the DNA surface followed by DNA-DNA attraction by bridging. It was found that negatively charged crowders compete with DNA for the binding of CTAB (at varying degrees), however, such competitive binding was much reduced when compact and spherical-like polyanions were used. This work does suggest that while negatively charged linear macromolecules are expected to compete with the DNA for proteins with low specificity and affinity, leading to the decompaction of DNA, spherical-like macromolecules or macromolecular complexes, such as ribosomes, do not interfere and can even potentially contribute to the DNA condensation and nucleoid formation.

6.2 Suggestion for future work

The findings suggest that adding PAMAM-OH interfers less with the interaction between DNA and CTAB than PMANa. In future work one should therefore use a negatively charged linear crowder, which has a similar charge and molecular weight as the dendrimers, to investigate if these findings are an effect of the charge and/or the shape of the crowders. Seeing as an increased effect on DNA condensation by CTAB was observed when increasing the concentration of PAMAM-OH dendrimers, one could assume that further increase could enhance DNA condensation above a certain crowder concentration. Therefore, future work should investigate the effects of increased crowder concentration, perhaps to something more similar to the concentration of macromolecules in bacteria cell, as well as investigations employing various other spherical-like macromolecules. It would also be benefitial to test other fluorescent dyes to find one that is less sensitive to the presence of the crowders at low ionic strength.

While aiding in understanding some of the phenomena observed in the experimental work, the results from Monte Carlo simulation were not very aligned with the experimental

ones. A few reasons contributed to this. Firstly, the obtained DNA-CTAB complexes were probably not at the lower energy configurations and, secondly the crowder molecules were not added to a pre-formed complex as in the experimental work. While the latter might not be very relevant, the former made it very difficult to compare the different systems, particularly the size distributions. These systems will benefit from longer runs, including more efficient Monte Carlo moves and/or annealing procedures to improve equilibration.

Bibliography

[1] G. Piekarski. Cytologische untersuchungen an paratyphus-und colibakterien. *Archiv. Mikrobiol.*, 8:428–439, 1937.

[2] L. Daneo-Moore, D. Dicker, and M.L. Higgins. Structure of the nucleoid in cells of streptococcus faecalis. *J. Bacteriol*, 141(2):928–937, 1980.

[3] J.A.C. Valkenburg and C.L. Woldringh. Phase separation between nucleoid and cytoplasm in *Escherichia coli* as defined by immersive refractometry. *J. Bacteriol*, 160(3):1151–1157, 1984.

[4] V.A. Bloomfield. DNA condensation by multivalent cations. *Biopolymers*, 44(3):269–282, 1997.

[5] R. de Vries. DNA condensation in bacteria: Interplay between macromolecular crowding and nucleoid proteins. *Biochimie*, 92(12):1715–1721, 2010.

[6] C.L. Woldringh and N. Nanninga. Organization of the nucleoplasm in *Escherichia coli* visualized by phase-contrast light microscopy, freeze fracturing, and thin sectioning. *J. Bacteriol*, 127(3):1455–1464, 1976.

[7] S.B. Zimmerman and A.P. Minton. Macromolecular crowding: Biochemical, biophysical, and physiological consequences. *Annu. Rev. Biophys. Biomol. Struct.*, 22:27–65, 1993.

[8] Y. Wang, M. Sarkar, A.E. Smith, A.S. Krois, and G.J. Pielak. Macromolecular crowding and protein stability. *J. Am. Chem. Soc.*, 134(40):16614–16618, 2012.

[9] K. Richter, M. Nessling, and P. Lichter. Macromolecular crowding and its potential impact on nuclear function. *Biochimica et Biophysica Acta*, 1783(11):2100–2107, 2008.

[10] S.B. Zimmerman and S.O. Trach. Estimation of macromolecule concentrations and excluded volume effects for the cytoplasm of *Escherichia coli. J. Mol. Biol.*, 222:599–620, 1991.

[11] A.J. Link, K. Robison, and G.M. Church. Comparing the predicted and observed properties of proteins encoded in the genome of *Escherichia coli* K-12. *Electrophoresis*, 18:1259–1313, 1997.

[12] J.D. Watson and F.H.C. Crick. Molecular structure of nucleic acids: A structure for deoxyribose nucleic acid. *Nature*, 171:737–738, 1953.

[13] Z. Guo, C.H. Taubes, J-E. Oh, L.J. Maher III, and U. Mohanty. DNA on a tube: Electrostatic contribution to stiffness. *J. Phys. Chem. B.*, 112(50):16163–16169, 2008.

[14] A. Pal and Y. Levy. Structure, stability and specificity of the binding of ssdna and ssrna with proteins. *PLoS Comput. Biol.*, 15(4):e1006768, 2019.

[15] S.B. Zimmerman and L.D. Murphy. Macromolecular crowding and the mandatory condensation of DNA in bacteria. *FEBS Letters*, 390:245–248, 1996.

[16] L. Guldbrand, B. Jönsson, H. Wennerström, and P. Linse. Electrical double layer forces. A Monte Carlo study. *J. Chem. Phys.*, 80:2221–2228, 1984.

[17] G. Maret. Magnetic birefringence study of the electrostatic and intrinsic persistence length of DNA. *Biopolymers*, 22:2727–2744, 1983.

[18] H-A. Tahmir-Riahi, M. Naoui, and R. Ahmad. The effect of Cu^{2+} and Pb^{2+} on the solution structure of calf thymus DNA: DNA condensation and denaturation studied by Fourier Transform IR difference spectroscopy. *Biopolymers*, 33:1819–1827, 1993.

[19] X-G. Sun, E-H. Cao, X y. Zhang, D. Liu, and C. Bai. The divalent cation-induced DNA condensation studied by atomic force microscopy and spectra analysis. *Inorg. Chem. Commun.*, 5:181–186, 2002.

[20] L.C. Gosule and J.A. Schellman. Compact form of DNA induced by spermidine. *Nature*, 259:333–335, 1976.

[21] D.K. Chattoraj, L.C. Gosule, and J.A. Schellman. DNA condensation with polyamines: Ii. Electron microscopic studies. *J. Mol. Biol.*, 121(3):327–337, 1978.

[22] J. Widom and R.L. Baldwin. Cation-induced toroidal condensation of DNA: Studies with $Co^{3+}(NH_3)_6$. *J. Mol. Biol*, 144(4):431–453, 1980.

[23] J. Widom and R.L. Baldwin. Monomolecular condensation of λ-DNA induced by cobalt hexammine. *Biopolymers*, 22(6):1595–1620, 1983.

[24] M. Joyeux. Compaction of bacterial genomic DNA: Clarifying the concepts. *J. Phys.: Condens. Matter*, 27:383001, 2015.

[25] M. Macvanin and S. Adhya. Architectural organization in *E. coli* nucleoid. *Biochim. Biophys. Acta*, 1819:830–835, 2012.

[26] R.T. Dame. The role of nucleoid-associated proteins in the organization and compaction of bacterial chromatin. *Mol. Microbiol.*, 56(4):858–870, 2005.

[27] D.E. Pettijohn. Histone-like proteins and bacterial chromosome structure. *J. Biol. Chem.*, 263(26):12793–12796, 1988.

[28] A. Travers and G. Muskhelishvili. Bacterial chromatin. *Curr. Opin. Genet. Dev.*, 15:507–514, 2005.

[29] J.N. Israelachvili, D.J. Mitchell, and B.W. Ninham. Theory of self-assembly of hydrocarbon amphiphiles into micelles and bilayers. *J. Chem. Soc., Faraday Trans. 2*, 72:1525–1568, 1976.

[30] J.C. Berg. *An Introduction to Interfaces and Colloids: The Bridge to Nanoscience*. World Scientific Publishing Company, 2009.

[31] S.M. Mel'nikov, M.O. Khan, B. Lindman, and B. Jönsson. Phase behavious of single DNA in mixed solvents. *J. Am. Chem. Soc.*, 121(6):1130–1136, 1999.

[32] R. Dias, S. Mel'nikov, B. Lindman, and M.G. Miguel. DNA phase behaviour in the presence of oppositely charged surfactants. *Langmuir*, 16:9577–9583, 2000.

[33] W.R. Will, P.J. Whitham, P.J. Reid, and F.C. Fang. Modulation of H-NS transcriptional silencing by magnesium. *Nucleic Acids Res.*, 46(11):5717–5725, 2018.

[34] R.T. Dame, C. Wyman, and N. Goosen. H-NS mediated compaction of DNA visualised by atomic force microscopy. *Nucleic Acids Res.*, 28(18):3504–3510, 2000.

[35] L.S. Lerman. A transition to a compact form of DNA in polymer solutions. *Proc. Nat. Acad. Sci. USA*, 68(8):1886–1890, 1971.

[36] Y.M. Evdokimov, A.L. Platonov, A.S. Tikhonenko, and Y.M. Varshavsky. A compact form of double-stranded DNA in solution. *FEBS Lett*, 23(2):180–184, 1972.

[37] A.P. Minton. Excluded volume as a determinant of macromolecular structure and reactivity. *Biopolymers*, 20(10):2093–2120, 1981.

[38] L.D. Murphy and S.B. Zimmerman. Macromolecular crowding effects on the interaction of dna with *Escherichia coli* DNA-binding protein: a model for bacterial nucleoid stabilization. *Biochim. Biophys. Acta*, 1219:277–284, 1994.

[39] C.F. Jordan, L.S. Lerman, and J.H. Venable. Structure and circular dichroism of DNA in concentrated polymer solutions. *Nat. New Biol.*, 236:67–70, 1972.

[40] M.K. Krotova, V.V. Vasilevskaya, N. Makita, K. Yoshikawa, and A.R. Khokhlov. DNA compaction in a crowded environment with negatively charged proteins. *Phys. Rev. Lett.*, 105:128302, 2010.

[41] A. Zinchenko, K. Tsumoto, S. Murata, and K. Yoshikawa. Crowding by anionic nanoparticles causes DNA double-strand instability and compaction. *J. Phys. Chem. B.*, 118:1256–1262, 2014.

[42] U.K. Laemmli, J.R. Paulson, and V. Hitchins. Maturation of the head of bacteriophage T4. V. A possible DNA packaging mechanism: In vitro cleavage of the head proteins and the structure of the core of the polyhead. *J. Supramol. Struct.*, 2(2-4):276–301, 1974.

[43] Y. Ichiba and K. Yoshikawa. Single chain observation on collapse transition in giant DNA induced by negatively-charged polymer. *Biochem. Biophys. Res. Commun.*, 242:441–445, 1998.

[44] M. Joyeux. A segregative phase separation scenario of the formation of the bacterial nucleoid. *Soft Matter*, 14:7368–7381, 2018.

[45] D. Frenkel and B. Smit. *Understanding molecular simulation*. Academic Press, 2002.

[46] N. Metropolis, A.W. Rosenbluth, M.N. Rosenbluth, and A.H. Teller. Equation of state calculations by fast computing machines. *J. Chem. Phys.*, 21:1087–1092, 1953.

[47] D.F. Evans and H. Wennerström. *The colloidal domain*. New York, NY: VCH Publishers, 1994.

[48] P.K. Maiti, T. Çağın, G. Wang, and W.A. Goddard. Structure of PAMAM dendrimers: Generations 1 through 11. *Macromolecules*, 37:6236–6254, 2004.

[49] M.P. Allen and D.J. Tildesley. *Computer simulation of liquids*. Claredon press: Oxford, 1987.

[50] J. Rescic and P. Linse. MOLSIM: A modular molecular simulation software. *J. Comput. Chem*, 36(16):1259–1274, 2015.

[51] M.E.J. Newman and G.T. Barkema. *Monte Carlo methods in statistical physics*. Oxford: Oxford University Press, Incorporated, 1999.

[52] M. Hof, V. Fidler, and R. Hutterer. *Fluorescence spectroscopy in biology*. Springer, Berlin, Heidelberg, 2005.

[53] K.E. van Holde, W.C. Johnson, and P.S. Ho. *Principles of physical biochemistry*. Prentice Hall, 2005.

[54] R.S. Dias, J. Innerlohinger, O. Glatter, M.G. Miguel, and B. Lindman. Coil-globule transition of DNA molecules induced by cationic surfactants: A dynamic light scattering study. *J. Phys. Chem. B*, 109(20):10458–10463, 2005.

[55] R.S. Dias, R. Svingen, B. Gustavsson, B. Lindman, M.G. Miguel, and B. Åkerman. Electrophoretic properties of complexes between dna and the cationic surfactant cetyltrimethylammonium bromide. *Electrophoresis*, 26:2908–2917, 2005.

[56] R.S. Dias and B. Lindman. *DNA interactions with polymers and surfactants*. John Wiley Sons, Inc., 2008.

[57] R.S. Dias, L.M. Magno, A.J.M. Valente, D. Das, P.K. Das, S. Maiti, M.G. Miguel, and B. Lindman. Interaction between DNA and cationic surfactants: Effect of DNA conformation and surfactant headgroup. *J. Phys. Chem. B*, 112:14446–14452, 2008.

[58] S.M. Mel'nikov, V.G. Sergeyev, and K. Yoshikawa. Discrete coil-globule transition of large DNA induced by cationic surfactant. *J. Am. Chem. Soc.*, 117:2401–2408, 1995.

[59] M-L. Ainalem, A. Bartles, J. Muck, R.S. Dias, A.M. Carnerup, D. Zink, and T. Nylander. DNA compaction induced by a cationic polymer or surfactant impact gene expression and DNA degradation. *PLos One.*, 9(3):e92692, 2014.

[60] S. Hou, K. Yang, and X-Z. Feng. Explanation for the electrophoresis behaviour of dna condensation induced by pseudopolyrotaxane of different lengths. *Electrophoresis*, 29:4391–4398, 2008.

[61] M. Pisarcik, F. Devinsky, and M. Pupak. Determination of micelle aggregation numbers of alkyltrimethylammonium bromide and sodium dodecyl sulfate surfactants using time-resolved fluorescence quenching. *Open Chem.*, 13:922–931, 2015.

[62] J.C. Brackman and J.B.F.N. Engberts. Influence of polymers on the micellization of cetyltrimethylammonium salts. *Langmuir*, 7:2097–2102, 1991.

[63] V.V. Vasilevskaya, A.R. Khokhlov, Y. Matsuzawa, and K. Yoshikawa. Collapse of single DNA molecule in poly(ethylene glycol) solutions. *J. Chem. Phys.*, 102:6595–6602, 1995.

[64] H. Kang, P.A. Pincus, C. Hyeon, and D. Thirumalai. Effects of macromolecular crowding on the collapse of biopolymers. *J. Phys. Rev. Let.*, 114:068303, 2015.

[65] K.A. Sharp. Analysis of the size dependence of macromolecular crowding shows that smaller is better. *Proc. Nat. Acad. Sci. USA*, 112(26):7990–7995, 2015.

[66] U. Kaatze, O. Göttmann, R. Podbielski, R. Pottel, and U. Terveer. Dielectric relaxation in aqueous solutions of some oxygen-containing linear hydrocarbon polymers. *J. Phys. Chem.*, 82(1):112–120, 1978.

[67] Y. Sasaki, D. Miyoshi, and N. Sugimoto. Regulation of DNA nucleases by molecular crowding. *Nucleic Acids Res.*, 35(12):4086–4093, 2007.

[68] R.S. Dias. Role of protein self-association on DNA condensation and nucleoid stability in a bacterial cell model. *Polymers*, 11(7):1102, 2019.

[69] S.K. Ramisetty and R.S. Dias. Synergistic role of DNA-binding protein and macromolecular crowding on DNA condensation. An experimental and theoretical approach. *J. Mol. Liq.*, 210:64–73, 2015.

[70] B. Tajik, B. Sohrabi, R. Amani, and S.M. Hashemianzadeh. The study of polymer-surfactant interaction in cationic surfactant mixtures. *Colloids and Surfaces A: Physicochem. Eng. Aspects*, 436:890–897, 2013.

[71] D. Chu and J.K. Thomas. Effect of cationic surfactants on the conformational transition of poly(methacrylic acid). *J. Am. Chem. Soc.*, 108:6270–6276, 1986.

[72] R.W. Wilson and V.A. Bloomfield. Counterion-induced condensation of deoxyribonucleic acid. A light-scattering study. *Biochemistry*, 18(11):2192–2196, 1979.

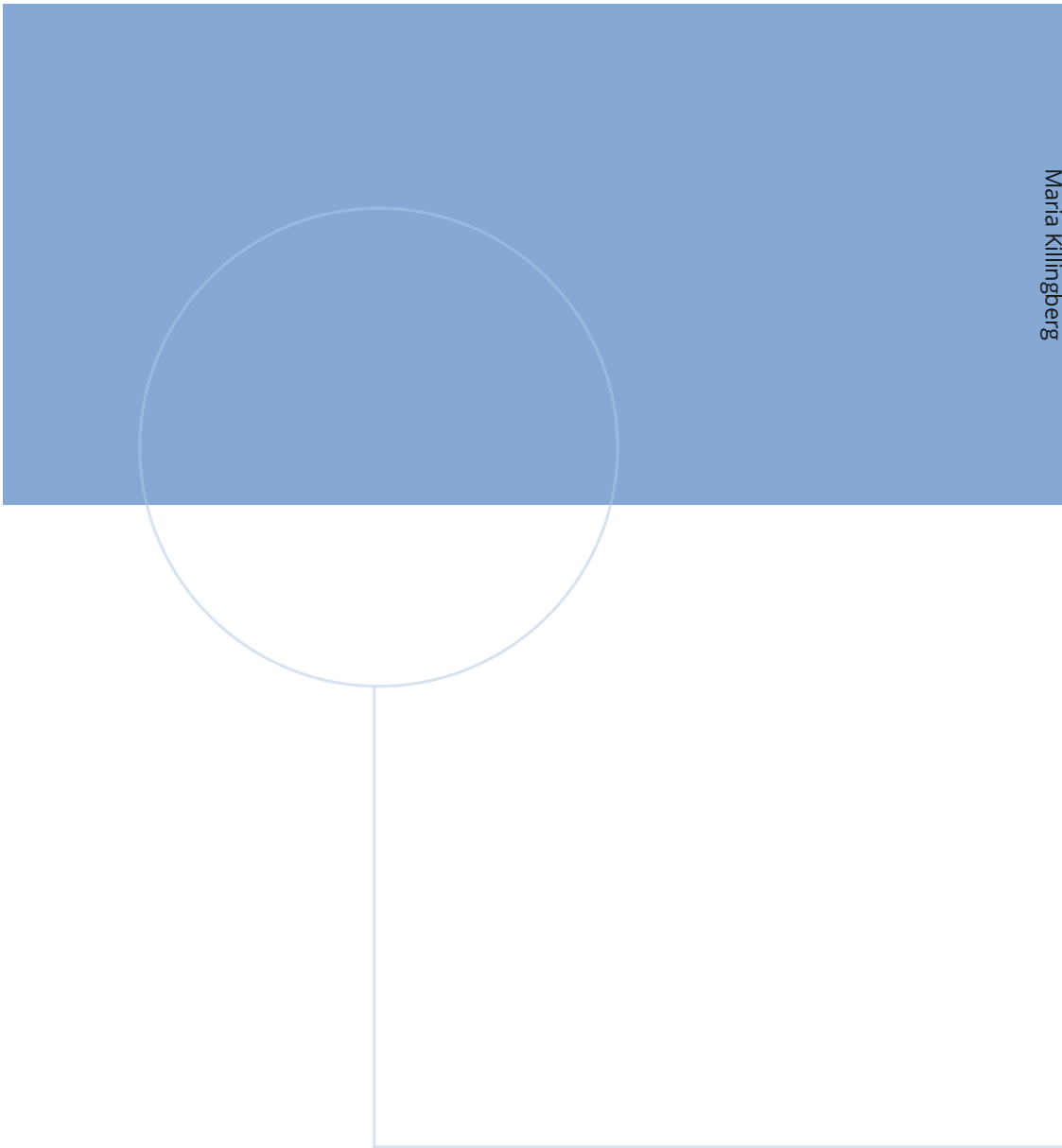

Maria Killingberg

NTNU
Norwegian University of
Science and Technology